Theoretical and Experimental Investigation of out-of-plane Wrinkle Formation during Steering in Automated Fiber Placement

Muhsan Milad Belhaj

A Thesis

In the Department

of

Mechanical, Industrial & Aerospace Engineering (MIAE)

Presented in Partial Fulfilment of the Requirements

for the Degree of

Doctor of Philosophy (Mechanical Engineering) at

Concordia University

Montreal, Quebec, Canada

January 2021

CONCORDIA UNIVERSITY

School of Graduate Studies

This is to certify that the thesis prepared

By: **Muhsan Milad Belhaj**

Entitled: **Theoretical and Experimental Investigation of out-of-plane Wrinkle Formation during Steering in Automated Fiber Placement**

and submitted in partial fulfillment of the requirements for the degree of

Doctor of Philosophy (Mechanical Engineering)

Complies with the regulations of the University and meets the accepted standards with respect to originality and quality.

Signed by the final Examining Committee:

_____ Chair
Dr. Hovhannes Harutyunyan

_____ External Examiner
Dr. Gangadhara Prusty

_____ External to Program
Dr. Khaled Galal

_____ Examiner
Dr. Van Suong Hoa

_____ Examiner
Dr. Farjad Shadmehri

_____ Supervisor
Dr. Mehdi Hojjati

Approved by: Dr. Martin D. Pugh, Chair
Department of Mechanical, Industrial & Aerospace Engineering

January 13, 2021 Dr. Mourad Debbabi, Interim Dean
Gina Cody School of Engineering and Computer Science

Abstract

Theoretical and Experimental Investigation of out-of-plane Wrinkle Formation during Steering in Automated Fiber Placement

Muhsan Milad Belhaj, Ph.D.

Concordia University, 2021

Automated fiber placement is being widely applied in the aerospace industry due to its advantages. This technology has the capability to improve the efficiency of composite structures by steering where properties such as stiffness can vary within the same part. However, steering is limited by process-induced defects such as out-of-plane wrinkles, which occur when the steering radius exceeds its critical limit. This thesis proposes a theoretical model for wrinkle formation during steering of the autoclave thermosetting prepreg. The Rayleigh-Ritz approach is used to model wrinkle formation based on the critical buckling load. The prepreg tape is considered an orthotropic plate resting on a Pasternak elastic foundation, which consists of one elastic spring layer connected to an elastic shear layer. Closed-form solutions for predicting both critical steering radius and buckling wavelength is presented. The two foundation parameters and the required mechanical properties of the prepreg are experimentally characterized. The model-predicted results are validated by the experimental results. The results reveal good agreement between the predicted and experimental values. It is also found that a significant improvement in the model was achieved by adding the shear layer to the foundation.

In this context, Normal stiffness of the foundation (prepreg tackiness) is demonstrated an important role in the AFP process and steering limitations. The second stage of this work aims to

measure the prepreg tackiness at different AFP processing conditions to study the effect of the process parameters on prepreg tackiness. Finally, this experimental work is used to predict the optimum parameters for high tackiness levels. Two in-house setups were developed for layup and measuring tackiness. The first setup was designed to simulate the AFP process and precisely control layup speed, compaction force, and temperature. It is used to layup the prepreg under different conditions and with different rollers. The second setup performs a peel-off test to measure the sample's tackiness. Taguchi method is applied to optimize the layup process parameters and find the optimal combination for high resultant tackiness. It is also applied to study the effect of the placing roller. Analysis of results shows that prepreg tack is affected by the interaction among the process parameters rather than the individual effect of these parameters. The study shows that the Taguchi method is suitable to solve the stated problem with a minimum number of trials as its results are experimentally validated.

Acknowledgments

First and foremost, I praise and thank Allah for His greatness and for giving me the strength and courage to complete this thesis.

I would like to express my deepest appreciation and gratitude to Dr. Mehdi Hojjati, for his guidance, patience and support throughout this program at Concordia University. This dissertation would not have been possible without his help. I would also like to thank Jeffrey Fortin-Simpson and Dr. Daniel Rosca for their technical support and guidance throughout the experimental work. My gratefulness extends to all my friends and colleagues, Dr. Hassan, Sam, Ali and Mohammad Hossein for their help and collaboration.

I would like to take this opportunity to thank the Ministry of Higher Education and Scientific Research in Libya for their financial support. I also want to thank Concordia Center for Composite (CONCOM) for all research facilities they have provided to accomplish this work.

My sincerest thanks to my parents, brothers and sisters for their endless love, support and encouragement throughout this long journey.

Finally, special thanks go to my wife (Salma) and my children (Nehal, Ahmed & Adam) for their patience, love and support.

Dedication

To my parents

The reason of what I become today.

Thanks for your great support, prayers and continuous care.

To my wife and my kids

You have been my inspiration.

Thanks for your endless love, patience, sacrifices, and support.

Table of Contents

List of Tables

List of Figures

Chapter 1: Introduction

In this chapter, we introduce the background of this research, which falls in the area of manufacturing of composite materials using automated fiber placement (AFP). More precisely, it is concerned with steering as a unique technique, which can be executed by AFP and its process induced defects. We also identify the motivations, problem statement, and research questions that we address in this thesis. Then, we list our objectives and discuss our methodology. Finally, we conclude this chapter by providing the thesis outline.

1.1 Background and Motivation

Composites are a material commonly composed of fiber reinforcements bonded together with a matrix material. The usage of composite materials has been significantly increased in the aerospace industry during the last three decades. Figure 1.1 shows how much composite materials have been used in Boeing airplanes over the last fifty years. Advanced composite materials constitute more than 50% of the weight of Boeing 787 and Airbus A350XWB. Composite materials are also in interest in other industries such as space, automobile, energy, biomedical and construction. This high demand of composite materials based on carbon fiber-reinforced polymers in the industry is due to its favorable mechanical and chemical properties. These properties include [1]:

- High strength
- Low density
- High stiffness
- Good fatigue resistance
- Good creep resistance
- Chemical resistance

- Low friction coefficient and good wear resistance
- Vibration damping ability
- Corrosion resistance
- High thermal conductivity
- Low electrical resistivity

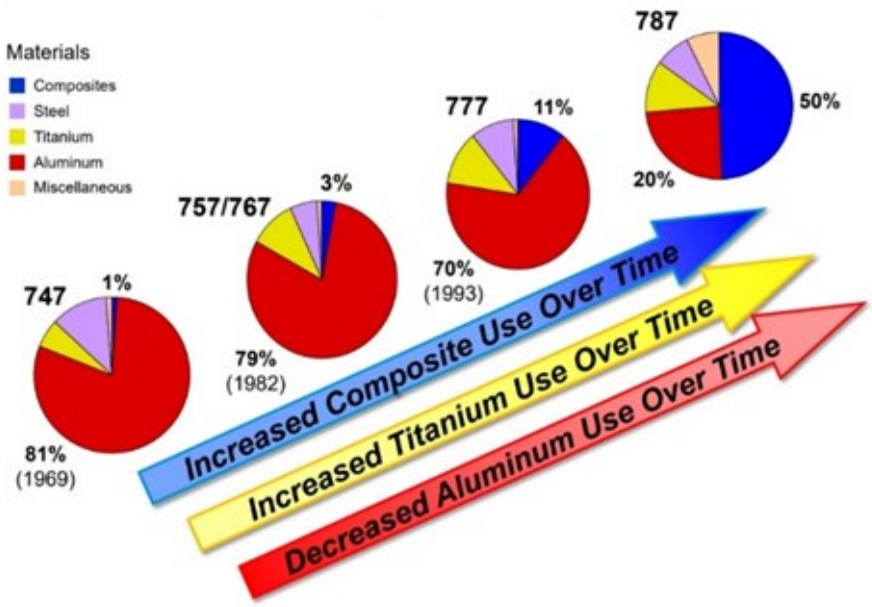

Figure 1.1. Materials used in Boeing planes 1969-2013 [2].

Manufacturing of carbon fiber-reinforced polymers (CFRPs) began with a simple process called wet hand layup (Figure 1.2), which is applicable for making a wide variety of different sizes of composite products. In this process, fibers reinforcements are manually placed on the mold. Subsequently, the resin is applied to the fibers by pouring, spraying or using a paint roller. Then, a hard roller (normally FRP roller) is applied on the reinforcements to consolidate the laminate, wetting the entire material and removing the entrapped air. Subsequent layers of the fiber reinforcement are added with the same direction or with different stacking sequence using the

same procedure to achieve the required laminate thickness. Prepreg materials can also be used in a similar manufacturing process called dry hand layup. Prepregs are composite materials in which the reinforcing fibers are pre-impregnated with partially cured resin system (typically epoxy). Prepreg reinforcements can be a unidirectional fibers or fabric. Using prepreg materials can significantly improve the part quality with better conformity and good control of laminate thickness. In hand lay-up process, final part quality is dependent on the skills of the operator which can affect the repeatability and quality consistency. Moreover Hand layup processes is limited by some drawbacks such as time-consuming, low in productivity, labor intensive and environmental issues related to the chemical emissions from the resin [3].

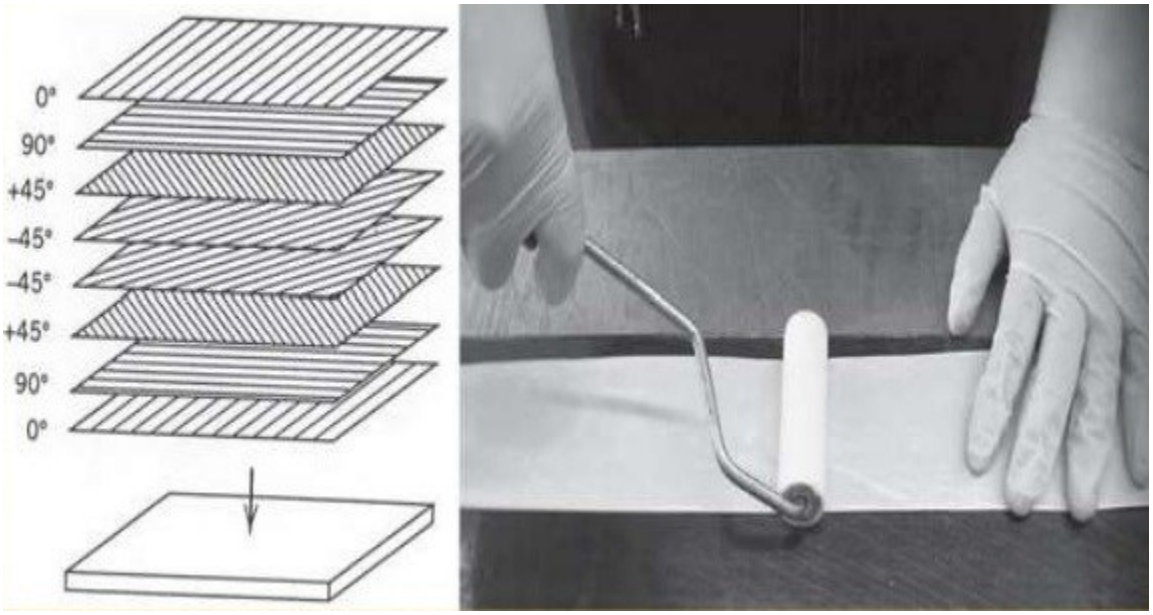

Figure 1.2. Hand lay-up process [4]

Automated lay-up technologies including Automated tape lay-up (ATL) and Automated fiber placement (AFP) (Figure 1.3) have been introduced to the composites industry to satisfy the increasing demand of high-quality composite parts and replace the hand lay-up process. These technologies have multiple advantages over the traditional hand lay-up, such as rising productivity,

reduced labor intensity, less material waste, and enhanced uniformity. AFP has been used to manufacture large parts in the aerospace industry such as the aftbody section of Boeing 787 (Figure 1.4) AFP has the capacity to lay-up pre-impregnated tows (prepreg) on a curvilinear path, known as steering. Taking advantage of steering extends design flexibility by tailoring the mechanical properties within the same laminate to produce the well-known variable stiffness laminates. Steering also can be used to lay-up material on complex shapes double curved surfaces by steering the fibers away from the geodesic of the surface.

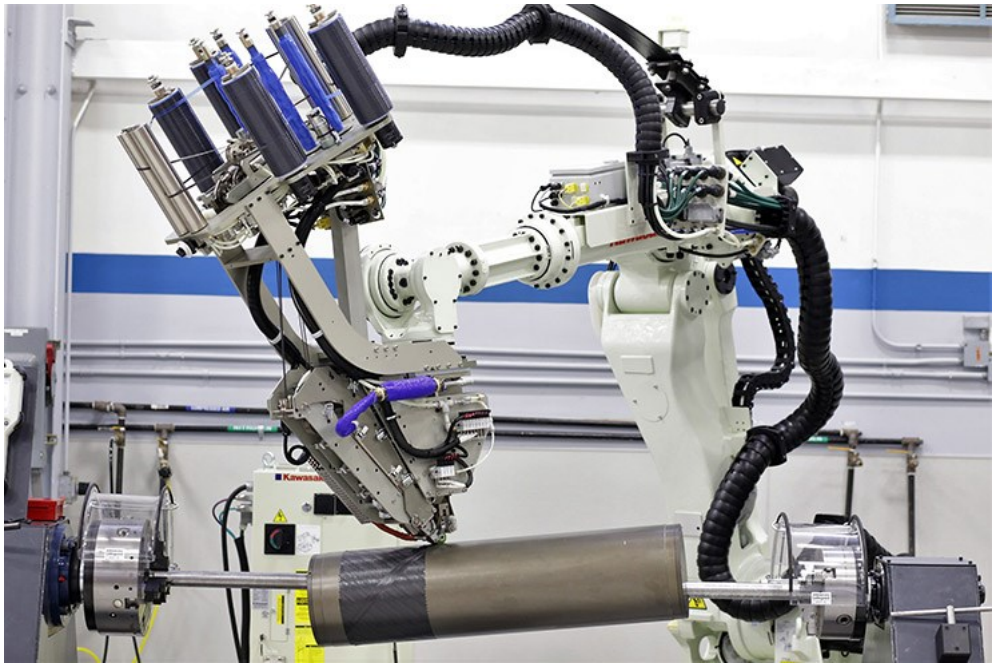

Figure 1.3. AFP from Automated dynamics [5]

Figure 1.4. Aftbody section of Boeing 787 manufactured by AFP [6]

Prepreg tack is defined as the ability of the prepreg to stick to the tool surface or adjacent layers. Prepreg tack is affected by different process and environmental parameters such as processing temperature, material deposition rate, compaction force and humidity. In the case of insufficient tack, prepreg may not stick on the prescribed path, which leads to a lay-up induced defects in the uncured laminates. These defects can significantly influence the performance of the final part.

In order to improve the degree of steering in AFP, which is the smallest possible radius fibers can be laid into without out-of-plane tow wrinkling, an accurate prediction of such defect should be reachable. Thus, designers should have a full understanding of steering including the material behavior and the interaction with process parameters. Moreover, the material properties and the process should be properly represented in the theoretical models. High prediction accuracy and awareness of the process limitations could significantly help designers and AFP technicians to properly choose the steering geometry, material, and process parameters. Consequently, reduce the time and cost spent on trial and error tests.

1.2 Objectives and Methodology

The main objectives of this research are:

- Determination of predicted critical steering radius using a two-parameter elastic foundation with shear layer counts for shear interaction between the spring elements.
- Validating the theoretical results by experimental work, which is performed using AFP machine.
- Experimental characterization of the foundation parameters, including normal and shear stiffness.
- Design a simple peel test to accurately measure the prepreg tackiness.
- Investigate the influence of the process parameters on prepreg tack and find the optimal combination of the process parameters.

As an improvement over existing solutions, this dissertation addresses the problem of out-of-plane wrinkles occur on thermoset prepreg when being steered by automated fiber placement (AFP). To achieve this objective, a new model of wrinkle formation was developed using Rayleigh-Ritz approach and based on the critical buckling load. The prepreg tape is considered as an orthotropic plate resting on a Pasternak elastic foundation, which consists of one elastic spring layer connected to an elastic shear layer. This model provided closed-form solutions to predict the critical steering radius as well as the wrinkles wavelength if the steering radius exceeds the critical one.

To validate this model, first, the two parameters represent the elastic foundation were experimentally characterized. A simple probe tack test was performed to characterize the normal stiffness, which counts for the tackiness between the prepreg and the substrate. The shear stiffness

was characterized by applying a bias extension test. Second, a set of different lay-ups with various steering radii were executed using a real AFP process to observe the existence of out-of-plane wrinkles and to measure the wavelength of the existing wrinkles. The closed-form solutions for critical steering radius and wrinkles wavelength were used to determine their values. These values were compared to their counterparts from the experimental work.

Finally, A new peel test setup was designed to measure tackiness between prepreg and substrate. Another setup was designed to lay-up peel test samples the way that AFP does. This lay-up setup has the capability to control the process parameters including, processing temperature, lay-up speed and compaction force. Therefore, the two setups were exploited to investigate the effect of each process parameter on tack level. Furthermore, we used Taguchi method to determine the optimal combination of process parameters that can be employed for a high tack level. This method was applied to reduce the high number of tests has to be done and save the time required to accomplish these tests.

1.3 Thesis Organization

In this outline, the remainder of this thesis is organized as follows: Chapter 2 provides A review of the relevant literature. Automated fiber placement (AFP) is presented along with steering and its induced defects. Out-of-plane wrinkles are discussed as one of these defects, and their available models are reviewed. Finally, prepreg tackiness and its characterization is briefly discussed. In chapter 3, the theoretical modelling of out-of-plane wrinkles is developed. The experimental work for foundation parameters characterization and the model validation is described. Finally, the comparison between experimental and theoretical results is discussed. In chapter 4, the two setups developed to automatically lay-up the samples and test them are presented. Taguchi method for

predicting the optimal conditions is described. Finally. Peel test results and effect of process parameters are discussed. Chapter 6 concludes this work and provides some hints for future directions.

Chapter 2: Literature Review

2.1 Automated Fiber Placement

Recently, fiber-reinforced composite materials have been increasingly used in the aerospace industry due to their superior variety of properties, such as low density, and high stiffness and strength. Different traditional manufacturing processes, such as hand lay-up have been used to produce different structures from composite materials. However, these manufacturing methods are limited by their shortcomings, including poor homogeneity, and high labor cost. Hence, development of new manufacturing processes has become a priority. Automated technologies have been introduced that use Automated Tape Laying (ATL) technology and Automated Fiber Placement (AFP) technology. These technologies have the ability to manufacture larger parts with high quality. AFP technology has been used in the aerospace industry to produce large curved composite parts of Boeing 787 and Airbus A350 Airplanes [7].

In the late 1980's, the first commercial AFP systems were presented, they were described as combined technology integrate filament winding and automated tape laying (ATL). This technology merges the differential tow payout capability of filament winding with the compaction and cut-restart capabilities of ATL technology. AFP is a process technology that manufactures high quality composite parts by a fully automated system. The functional principle of thermoset AFP is illustrated in Figure 2.1. A laminate is executed by laying-up multiple layers prepreg slit-tape on a double-curved substrate or tooling surface. The prepreg is pressed onto the substrate by a compaction roller. The substrate is heated by a heating source shortly before the nip-point, where the incoming prepreg comes into contact with the substrate. The prepreg's matrix is activated immediately through the substrate and becomes sticky. As the viscosity of the matrix decreases,

the prepreg tackiness increases and allows the prepreg to adhere to the substrate and increases the prepreg's formability. At the end of each ply, a cutting device is used to cut the prepreg and start another one [8]. A placement head is mounted onto a robot or a gantry unit based on the delivery system of the material to the placement head., The material is either fed to the head through a creel cabinet in the robotic type or stored directly on the head in the gantry units. Within the context of this thesis, the focus was on robotic fiber placement as most of the experimental work was done on a robotic AFP equipment by Automated Dynamics. Additional information on AFP technology can be found in the following references [7-12].

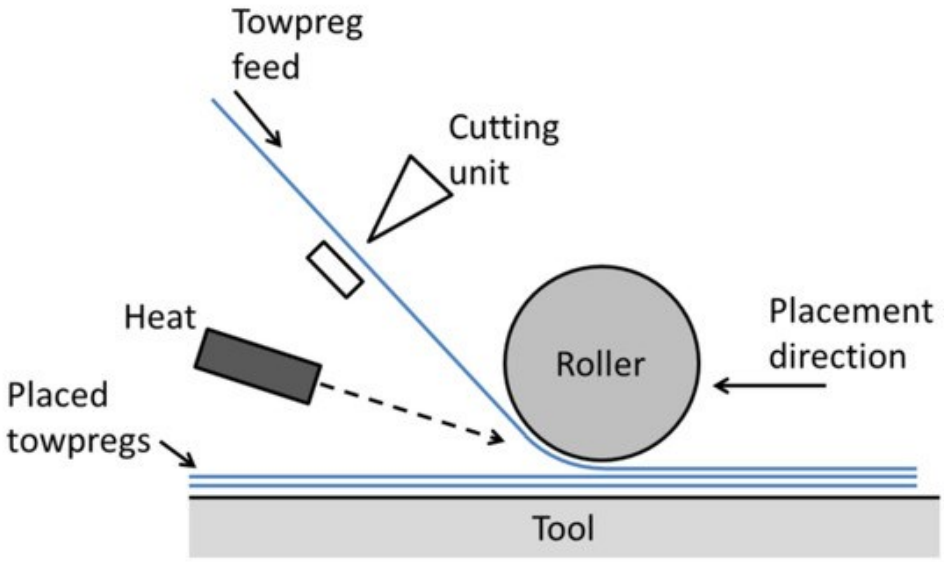

Figure 2.1. Schematic of the automated fiber placement process [14]

A typical thermoset AFP Placement head is depicted in Figure 2.2. The placement head can accommodate up to 32 tows forming a band called course with a tow width of 3.175–6.35 mm at linear speed up to 1 ms^{-1}. This placement head can cut and restart any individual tow during the lay-up process. The route of the prepreg during the whole process starts from the material supply unit (bobbins), which mounted on the head. The prepreg is guided into a tension control system

through a fiber guiding unit to keep the fibers straight and manage the dynamic effect of the process. The guiding system is separately cooled to a recommended temperature by the material supplier to prevent the prepreg from sticking to guiding system parts.

The compaction roller with a heating source provides the adhesion between the prepreg and the substrate. The heating source can be an infrared emitters, lasers, or hot gas torch. The latter is the most heat source adopted in the automated placement of composites. Most commonly, an elastic deformable compaction roller made from polyurethane or silicon is used in the thermoset AFP to elastically conform to the double curved surfaces and ramps. At the end of each course, each prepreg can be individually cut perpendicular to the lay-up direction and restarted. Knife edge or laser can be used in the cutting device. This device must be able to cut the individual prepreg at any time during the lay-up process without deceleration. The cutting quality is negatively affected by increasing the deposition rate, which requires additional operations on the uncured produced part [15].

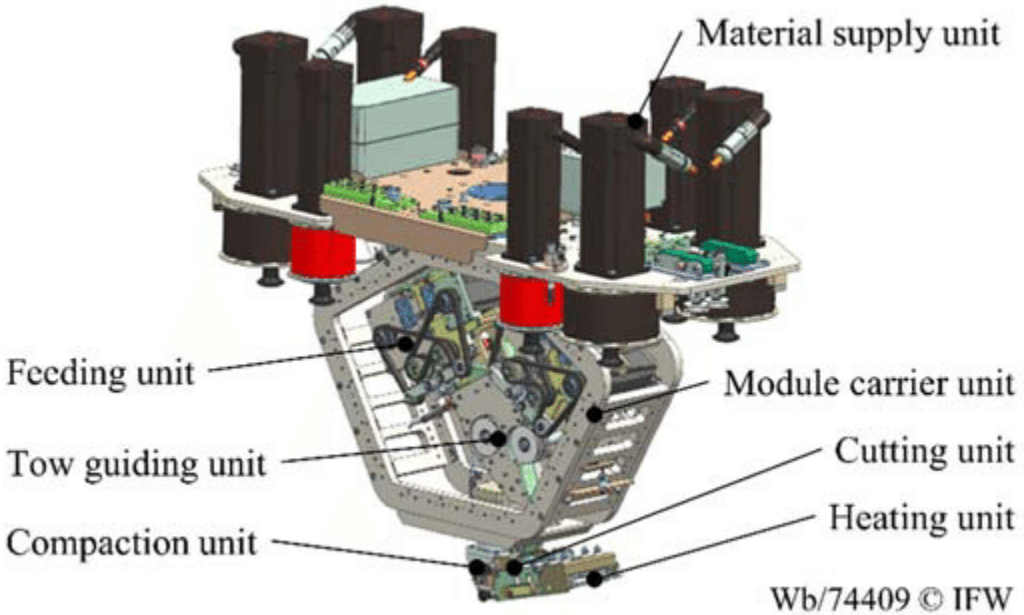

Figure 2.2. AFP thermoset placement head [16]

The composite material laid-up by AFP can either be impregnated tows or slit prepreg tape. The latter is more expensive due to its productivity, reliability, and product quality. They both are normally wound onto cardboard bobbins and supplied with an interleaf film to prevent tack and friction in the material supply. The small diameter of the bobbin can improve the tension control accuracy during unwinding [17].

Automated fiber placement is being widely applied in the aerospace industry due to its advantages, which include high-quality parts, Higher productivity, low labor force and minimum of the number of the required parts. The ability of laying-up the tows with deferent speeds, with each tow can be cut and restart individually makes AFP a unique technology to execute complex composite structures. Steering is also can be performed by exploiting the differential tow pay-out capability. Steering by AFP increases the design flexibility by varying the mechanical properties within the same part using the curvilinear path, thus, producing optimal composite structures [6, 17, 18].

2.2 Variable Stiffness Laminates

By using fiber placement technology, the fibers in each ply can be steered in curved paths that allow the mechanical properties to vary from one point to another over the structure, which is defined as “Variable Stiffness Laminates” [20]. There are two methods to make a complete ply of variable stiffness laminate. The first one is the shifted fiber method, where the first laid-up fiber path is the reference one, and the next path is generated by shifting an identical copy of the reference path by a fixed distance normal to the variation direction. causing a combination of gaps and overlaps [21]. The second method is the parallel method. In this method, the courses are laid up parallel to the reference path with the same distances between the courses along the whole

trajectory [22]. In this method, the fiber orientation changes to keep the constant distance from the reference path, which results in a uniform thickness with no gaps and overlaps. However, at a certain distance from the reference path, small steering radii cannot be steered as they reach the allowable steering radius [23]. The two configurations are depicted in Figure 2.3.

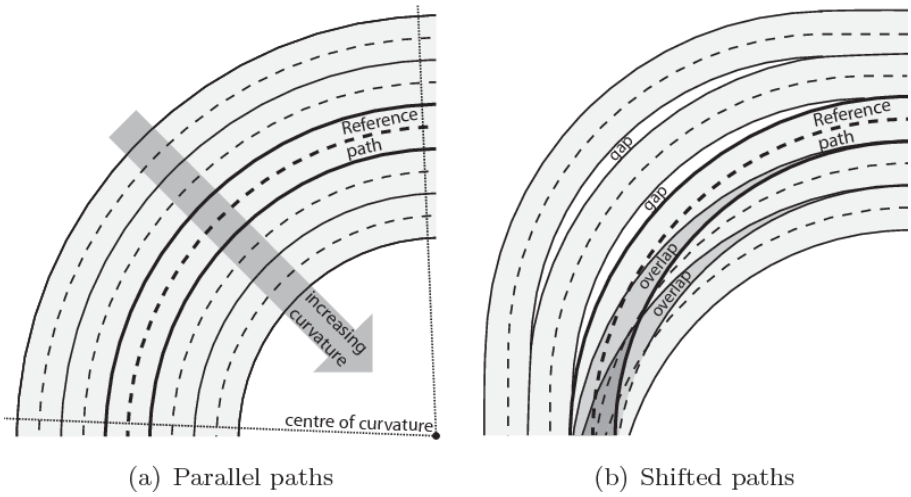

Figure 2.3. Tow paths derived from a reference curve [23]

Several studies have been done to demonstrate the advantages of variable stiffness panels over their conventional counterparts. A numerical model was developed by Gurdal and Olmedo [20] to study the elastic behavior of variable stiffness panels. They reported that variable stiffness laminates have an axial stiffness up to 50% higher than the constant stiffness laminates. The same work was extended to study the buckling load of variable stiffness panels [24]. Two different orientations were considered, with the fiber orientation varies in the direction of the applied load and perpendicular to it. Both cases showed increase in buckling load up to 80% higher in the case with the fiber orientation varies perpendicular to the applied load compared to conventional laminates. Similarly, Rouhi et al. [25] used a multistep design optimization process to design and optimize a steered composite cylinder for critical buckling load under only bending loading. The

radius and aspect ratio (length/radius) were investigated as structural parameters. An improvement of the buckling load up to 38.5% was reported for variable stiffness cylinder with low aspect ratio values. However, the effect of the radius was not as great as that of aspect ratio. In addition, they reported that with the same dimensions, steered cylinder had a buckling load improvement up to 24.8% compared to its quasi-isotropic counterpart. This improvement referred to the efficient load distribution achieved by steering. Moreover, the same authors [26] extended their work to examine how such buckling load improvement would be affected by changing the load direction.

In different study, variable stiffness panels with different sizes of holes were tested under compressive and shear loads. The obtained results showed a marked improvement in the failure performance of the curvilinear panels up to 60% over straight fibers laminates [27]. Furthermore, a study was done by Lopes et.al [20, 27] considering the compressive buckling and first-ply failure loads. In this study the first-ply failure of steered panels was remarkably improved compared to traditional straight laminates. More examples of performance improvement are reviewed by Lopes [29], Fagiano [30], and Peeters et.al [31]. Clancy et.al [32] experimentally studied the ability of AFP to lay-up a variable stiffness laminate using carbon fiber (CF)/polyetheretherketone (PEEK) tapes. They reported that thermoplastic variable stiffness laminates can be successfully steered by AFP with small steering radii.

2.3 Lay-up Defects Caused by Steering

Various defects are generated during steering that must be considered during the design and manufacturing of steered laminates. These defects are divided into an individual level defects and course level defects. Individual defects arise from the mechanical deformation of each tape due to the curvilinear path lay-up. They include out-of-plane tape buckling (wrinkles), in-plane fiber

waviness, tape pull-off and tow misalignment as shown in Figure 2.4. The course level defects occur due to the method (parallel, shifted) used to lay-up the steered bands to cover the hole laminate such as gaps and overlaps (Figure 2.3).

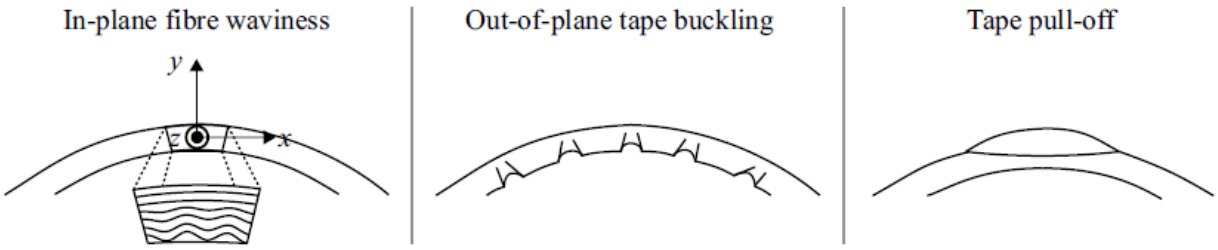

Figure 2.4. Tow steering defects (individual level) [33]

In-plane fiber waviness take place in the steered tapes in the form of in-plane sinusoidal disorientation from the principal direction of the fibers inside the tape. During steering, the prepreg is curved in the plane of the surface causing the inner radius to be under compression. Fibers under compression form the sinusoidal shape due to an elastic fiber micro-buckling [34]. On the other hand, tension on the outer radius of the steered tape generates tape pull-off. Out-of-plane tape buckling is the defect in interest of this thesis, which will be reviewed in the next section. Heinecke and Willberg [35] reviewed the manufacturing induced imperfections related to AFP process. They classified these imperfections to ten categories with more focus on gaps and overlaps.

Kim et al. [36] introduced a new technique called continuous tow shearing (Figure 2.5). Unlike the in-plane deformation used in current automated fiber placement machines, the in-plane shear deformation is applied to make the fiber tow follow the designed tow path. They reported that all the mentioned steering defects can be avoided using this technique.

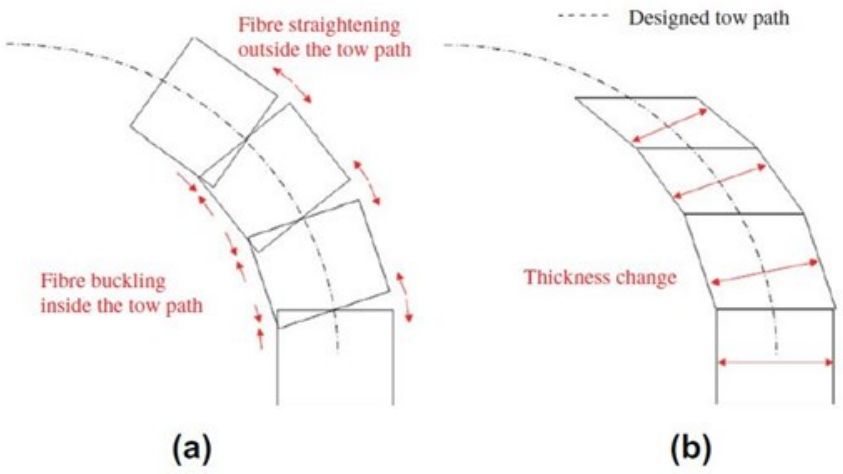

Figure 2.5. (a) Conventional AFP, and (b) CTS (Continuous Tow Shearing) [36]

2.3.1 Out-of-plane Buckling (Wrinkles)

Out-of-plane buckling is one of the main defects caused by fiber steering. It occurs on the inner radius of the steered tow due to the excessive compression load generated from the difference of length between the steered fibers and the curvilinear path. When the steering radius exceeds its critical value, the adhesive forces cannot hold the tapes, which in turn split up from the substrate and buckle. These wrinkles restrain the application of steering by limiting the minimum steering radius, which can be laid-up with no wrinkles or other defects.

Wiehn and Hale [37] reported that automated fiber placement machine can lay-up tows with a minimum steering radius up to 50.8 cm. Another minimum turning radius (63.5 cm) was proposed by Negendra et al. [38] to avoid local fiber buckling. [39]. On the other hand, to evaluate the quality of the fiber path, a new criterion was proposed by Zhao et al. [40]. The quality of the fiber trajectory was evaluated by the comparison between the path geodesic radius and the critical buckling radius. Good lay-up quality is achieved when the path geodesic radius is larger than the critical buckling radius.

2.3.2 The Effect of Fiber Waviness

Fiber waviness generated from in-plane and out-of-plane buckling during placement of prepreg causes a geometrical inhomogeneity, which impact the mechanical performance of the final product. In the literature, different approaches were reported to study that impact with more focus on the effect of fiber waviness arises from out-of-plane buckling.

Hsiao and Daniel [41] developed a theoretical models to study the influence of fiber waviness on stiffness and strength of unidirectional composite laminates subjected to compression loading. To verify the analytical results, a compression tests were performed. The results indicated a significant decline in both young's modulus and compressive strength due to the existence of fiber waviness. Moreover, they observed that interlaminar shear failure was the controlling failure mechanism in the conducted tests. Furthermore, Caiazzo et al. [42] mentioned that the amount of the effect depends on location and size of fiber waviness regions. Bogetti et al. [43] indicated that out-of-plane fiber waviness may also create high interlaminar shear stress that decreases compression strength.

El-Hajjar and Peterson [44] investigated the tension behavior of unidirectional and multidirectional laminates containing three levels of ply waviness. They reported a great impact on stiffness and strength. Similarly, Garnich and Karami [45] referred the significant decrease of strength to local longitudinal shear and transverse normal stresses that caused by fiber waviness. Lastly, the impact of ply waviness on fatigue life of tapered flexbeam laminates was investigated by Murri [46]. The tested samples with varying levels of waviness through the thickness were subjected to both axial tension and transverse bending loads. The author concluded that failure started with cracks through the waviness areas before the cracks expanded to delamination in both directions. Compared to tested samples without ply waviness, samples having ply waviness were

shown a great shorter fatigue life. Additional studies on the influence of fiber waviness can be found in [46-51].

2.3.3 Modelling of Prepreg Wrinkling During Steering

Beakou et al. [53] developed the first model considering the out-of-plane buckling of uncured prepreg during steering by AFP. In this model, the individual wrinkles were represented as an orthotropic plate under in-plane load (Figure 2.6). This plate is resting on independent spring elements foundation, which represents the interaction between the material and the substrate (tackiness). The plate assumed to have one free edge where the buckling is generated and three simply supported edges. The critical buckling load was determined by using Ritz method and the minimum radius of curvature was determined by using the relation between the bending moment and the curvature as following.

$$\frac{1}{r} = \frac{d^2y}{dx^2} = \frac{M_z}{E_1 I} \tag{2.1}$$

$$M_z = \frac{\alpha N_{o_{cr}} b^2}{48} \tag{2.2}$$

$$r = \frac{E_1 bh}{2\alpha N_{o_{cr}}} \tag{2.3}$$

Where E_1 is longitudinal young's modulus of the tow, I is second moment of area of the tow cross section, M_z is the bending moment, b is tape width, r is the steering radius, α is a load parameter, $N_{o_{cr}}$ is the critical buckling load, and h is tape thickness.

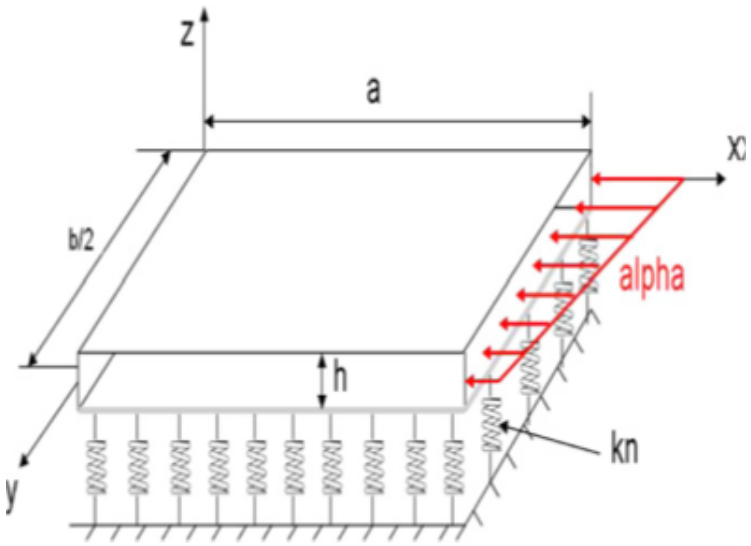

Figure 2.6. Anisotropic plate on one-parameter elastic foundation [53]

Matveev et al. [54] introduced another model for the same purpose, they used the same material and foundation representation with different boundary conditions. The orthotropic plate in this model has two clamped sides, one simply supported edge and one free edge for the buckled side. These boundary conditions provided more accurate representation of the real process as depicted in Figure 2.7. They also used Ritz method to determine the critical buckling load, which used to identify the critical steering radius. The two models will be more reviewed in the next chapter. Recently, Wehbe et al. [55] developed a geometrical model using a simple form of a wrinkled shape (Figure 2.8) to investigate the out-of-plane wrinkles during AFP process. The amplitude of the wrinkles can b determined for a particular wrinkle wavelength, which can be either measured experimentally or obtained by the another mechanical model for wavelength determination as the one developed by Belhaj and Hojjati. [56]. Numerically, they found that higher amplitude of wrinkles is obtained when the prepreg width is increased. They also indicated that lower wrinkle amplitudes can result from rising the number of wrinkles within a defined path. Rajan et al. [57] applied a 3D Stereo Digital Image Correlation system (StereoDIC) to

experimentally investigate the out-of-plane and in-plane deformation on the prepreg laid-up by automated fiber placement. This image system provides a 3D full field displacement and strain, which facilitate the measurement the shape and deformation of the formed defects.

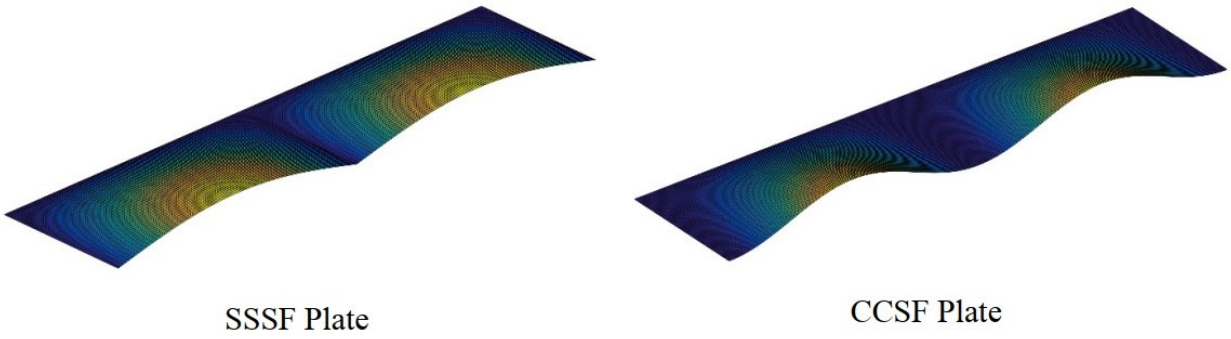

Figure 2.7. wrinkle formation with different boundary conditions [58]

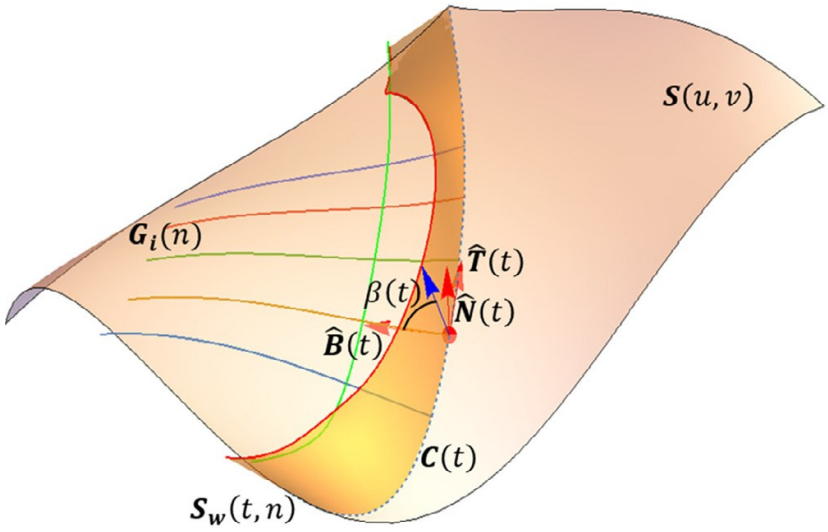

Figure 2.8. Schematic of a wrinkle on a general surface [55]

2.4 Prepreg Tack

Generally, tack can be defined as the sensation one experiences when removing his finger from an adhesive tape or any sticky material [59], this definition is more appropriate for adhesive tack. In composites, tack is the mechanical property measures the prepreg resistance from being detached from the substrate or the adjacent layers [60]. Prepreg tack is considered a crucial factor in Automated lay-up processes to successfully manufacture high-quality composite parts. Insufficient prepreg tack leads to a low-quality product with lay-up defects. It also can cause adhesion inside the placement head or on the placing roller, which leads to a failure of the lay-up machine. Prepreg tack is led by an interaction of two lay-up phenomena (adhesive and cohesive), which affected by process and environment parameters along with the inherent properties of the prepreg itself. Table 2.1 summarizes the factors that could affect prepreg tack during automated lay-up [61].

Table 2.1. AFP/ATL-related influences on prepreg tack [61]

Category	**Influence parameter**	**Description**
Process parameter (extrinsic)	Temperature	Prepreg, head, and mold temperature
	Compaction force	Pressure on material at nip point applied by compaction roller
	Compaction time	Duration of compaction (dependent on lay-up speed)
	Debonding rate	Defect/lay-up speed-dependent rate of prepreg removal from substrate
	Contact material	Surface material in contact with prepreg (mold, roller, backing paper, etc.)
Environmental factor (extrinsic)	Ageing	Material storage in and out of freezer due to proceeding cure reaction
	Relative humidity	Relative humidity in manufacturing environment causing moisture pickup
Material property (intrinsic)	Matrix viscosity	Epoxy resin flowability
	Prepreg architecture	Structural composition (impregnation level, tack-enhancing resin layers, etc.)
	Fiber volume fraction	Volumetric fiber/resin ratio
	Degree of cure	Cured portion in initial B-stage as delivered

2.4.1 Prepreg Tack Measurement

Although prepreg tack plays an important role in composite manufacturing by automated fiber placement, this property has not properly been identified by the suppliers through the material data sheets. The only information provided is classifying the tack level into three different scales; low, medium and high or providing the time in which the material can maintain its tack level (tack life). To evaluate the prepreg tack in the industrial approach, a combination of practical methods with the experience is used. For instance, the prepreg sample is placed on vertical support and the period of time the prepreg keeps attached to the supporter is used to identify how tacky the prepreg is [62]. In the literature, different methods have been exploited to characterize the prepreg tack. Most of these methods have been adapted from the pressure sensitive adhesives (PSA) industry due to their similar adhesive nature. Probe test and peel test have been mostly utilized for the measurement of prepreg tack, the two methods will be reviewed in the coming chapters.

A probe test technique was developed for the first time in the 1980s to study the prepreg tack as a function of contact time, pressure and of separation rate [63]. Dubois et al. [62] used the probe tack test with more advanced setup to investigate the tackiness of carbon/epoxy prepreg. The experiments were carried out by the same method used for pressure sensitive adhesives. Both pure resin and prepreg were tested. First, they reported that pure resin behavior was comparable to that of viscos silicon oil (Figure 2.9). Second, in the prepreg test, three samples were tested under the same conditions. Due to structural effects of the fiber, the response of the three samples was different and differs from that of pure resin (Figure 2.10). They investigated the effects of contact time and pressure, probe temperature and debonding rate on the prepreg tack. they found that debonding force decreases as the temperature increases, which was attributed to the change of the

resin properties. It was also reported that the maximum debonding force is proportional of the debonding rate.

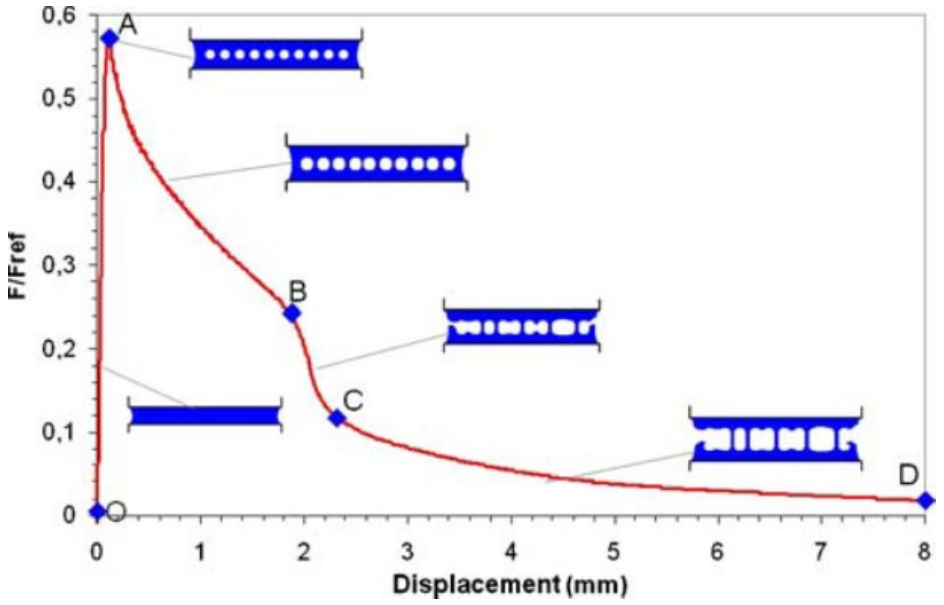

Figure 2.9. Force-displacement curve for resin M21 [62]

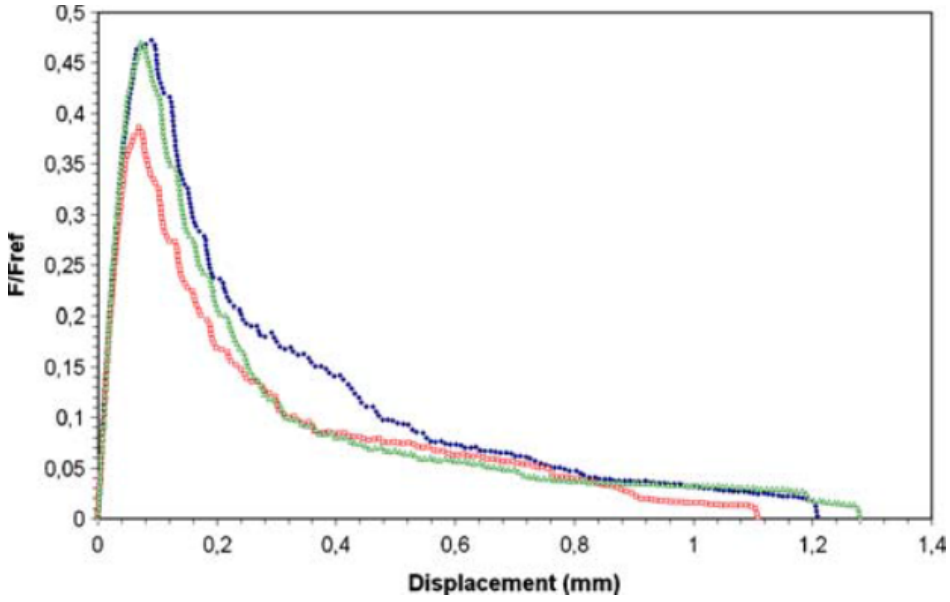

Figure 2.10. Force-displacement curves obtained for three prepreg samples [62]

For a better control of the experimental parameters, Wohl et al. [64] performed a probe test inside a rheometer. They reported a maximum tack value at moderate contact force values, which attributed to the movement of the resin from the contact area. Another maximum tack value was observed at medium relative humidity due to the viscoelastic behavior of the resin. Floating roller peel test was also used to characterize prepreg tack in concordance with ASTM D3167, which was originally developed to measure the tack of pressure sensitive adhesives [64 ,65]. A new peel test apparatus based on the floating roller method was introduced by Crossley et al. [67] to measure the tackiness and dynamic stiffness of prepreg. The test machine was modified to imitate the process of ATL and AFP. As illustrated in Fig. 2.11, when the test was conducted on a specified medium tack prepreg samples, there was an obvious increase in the rolling resistance when the stiffness turns to peeling resistance. In addition, different values of tack and stiffness were obtained when commercial hand lay-up prepreg samples were distributed along the roll. Moreover, the obtained tack and stiffness values were differed from those specified by the manufacturers. Furthermore, different prepreg materials showed inconsistent response to temperature increase. This was referred to the interfacial and cohesive failure modes observed in low tack and high tack samples, respectively. The same apparatus was continuously used in different experimental investigations regarding prepreg tack [67‑69].

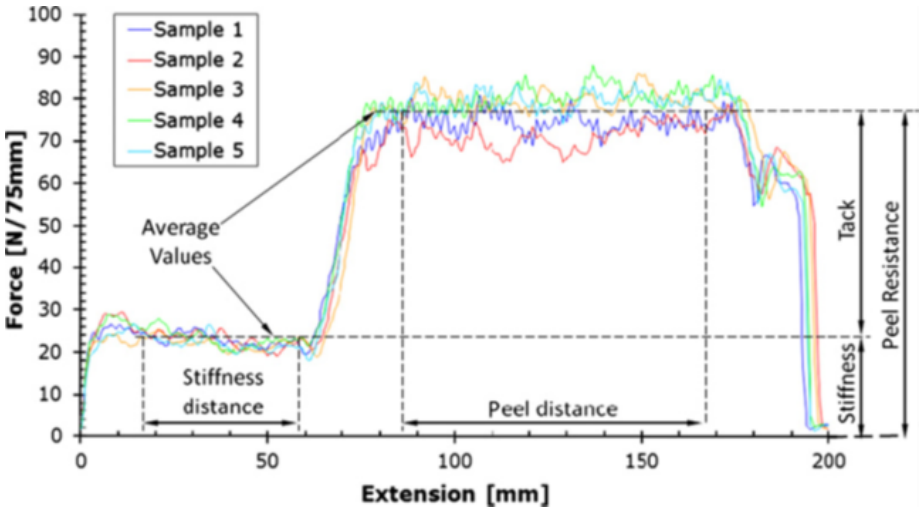

Figure 2.11. The recorded Stiffness and peel resistance for medium tack prepreg samples [67]

Chapter 3: Modelling and Experimental Validation

3.1 Introduction

Due to their improved characteristics over other traditional materials such as steel and aluminum, fiber-reinforced composite materials have been progressively utilized in the aviation industry. While a variety of structures can be produced through conventional manufacturing methods, including hand lay-up, these processes have several disadvantages, such as a high cost and a lack of consistency. Technologies based on automation, e.g., Automated Fiber Placement (AFP) and Automated Tape Laying (ATL), have enabled the high-quality manufacture of large composite products. Within the aviation industry specifically, Airbus and Boeing use AFP to produce the large parts made of composite materials in their latest aircraft [7].

AFP technology merges the differential tow payout capability of filament winding with the compaction and cut-restart capabilities of ATL technology. In the AFP process, individual prepreg tapes are fed into a fiber placement head through a fiber delivery system where they are collimated into a fiber band and laminated onto a mold surface [13] . The placement head of modern machines can accommodate up to 32 tows with a tow width of 3.175–6.35 mm at linear speed up to 1 ms^{-1}. This placement head can cut and restart any individual tow during the lay-up process. Thus, permitting the band width to widen or narrow in increments equal to one tow width, each tow of the band is dispensed at its own speed enabling fabrication of contoured surfaces and tow steering [7, 28].

By using fiber placement technology, the fibers in each ply can be steered in curved paths that allow the mechanical properties to vary from one point to another over the structure, which is defined as “Variable Stiffness Panels” [71]. These laminates remarkably increases the design

flexibility leading to higher structural performance compared to its classical counterpart [72]. Variable stiffness laminates show a remarkable improvement in terms of buckling load, first-ply failure, and strength performance [20, 27, 28, 70, 72]. However, steering of tapes produces some manufacturing defects. The main two defects of this process are out-of-plane wrinkling and tow pull-up. These defects occur at the inner and outer radii of the tow due to the excessive compression or tensile forces generated from the difference of length between the tow and the steering path [54]. As a result, they restrict the limitation of the steering radius and other process parameters. Different values of minimum steering radius have been reported in the literature. According to Wiehn and Hale [37], AFP machines can enable the layup of tows with a steering radius of no less than 50.8 cm to have steered tows with no wrinkles. Similarly, Negendra et al. [38] suggested using a radius of 63.5 cm to prevent the local buckling of the fibers. In addition, a decrease in the tow width to 1/8 inch from 1/4 inch reduced the radius by over 50% [39]. Meanwhile, Zhao et al. [40] put forward an additional criterion that could determine the fiber path quality. They demonstrated that comparing the radius of the geodesic path with the critical buckling radius facilitates an evaluation of the fiber trajectory quality. If the former is greater than the latter, then the layup is considered to have good quality.

Recently, two different models for the defect development during lay-up of curved tape were developed by Beakou et al. [53] and Matveev et al. [54]. Beakou's model defined the minimum steering radius of prepreg based on maximum buckling load. The second model introduced a closed form solution for the predicted minimum steering radius of dry fiber. These two models considered the material as an orthotropic plate resting on one parameter elastic foundation. This parameter represents the interaction between prepreg plies or prepreg ply and tool, which is known as tackiness. Beakou et al. [53] demonstrated that tackiness strongly affects the critical load, and

hence the minimum steering radius. In addition, Crossley et al. [66, 69] reported a non-linear behavior of prepreg tack as a function of lay-up temperature and speed of deformation. Moreover, Hormann [74] acknowledged that in addition to prepreg tackiness, the formation of out-of-plane tape buckling is significantly affected by the material shear modulus. Both models considered the influence of material tackiness on out-of-plane buckling by using spring elements to represent the elastic foundation and level of tackiness. Neither models, however, take into account the effect of shear layer, which assumes some kind of interaction between the spring elements. This condition will help in bringing the formulation closer to reality [75]. Therefore, the present work aims to study out-of-plane buckling (wrinkles) of a steered prepreg tape by adding a second parameter to the elastic foundation to account for the shear layer.

In this work, the Rayleigh-Ritz approach is used to model the wrinkles formation, in which the tape is considered as an orthotropic plate subjected to a non-uniform compressive load. The interaction between the plate and the substrate is presented by a Pasternak foundation with two parameters. The first parameter accounts for normal stiffness of the foundation, while the second parameter represents the shear stiffness. These parameters are experimentally characterized. A closed form solution for the predicted critical steering radius is obtained based on the critical buckling load. The effect of foundation parameters on the steering radius is presented. Experimental results are presented to validate the model in terms of the critical steering radius and the buckling wavelength.

3.2 Theoretical Formulation

To model the out-of-plane wrinkling during steering, the prepreg is considered as an orthotropic plate of length L, width b, and thickness h resting on Pasternak elastic foundation that consists of two layers; linear elastic spring layer of constant per unit area k (N/m^3), and a unit thickness shear layer of constant G (N/m) [76]. The plate is clamped at its two side edges, is free at its compressed edge, and is simply supported at the tensioned edge. The coordinate system is considered so that the origin is at one corner of the middle surface of the plate; x, y, and z coordinates are taken along the length, as shown in Figure 3.1.

The load applied on the plate is an in-plane bending caused by steering the prepreg tape into a curvilinear path. As a result, the tape is subjected to a non-uniform load described by a stress distribution factor α, which defines the position of the neutral plane between tensile and compressive stresses. Different values of factor α and the resulted stress distributions are illustrated in Figure 3.2. Due to the steering load, the value of α is expected to be between 1 and 2. In this study, we assumed that steering applies pure bending, hence α is equal to 2.

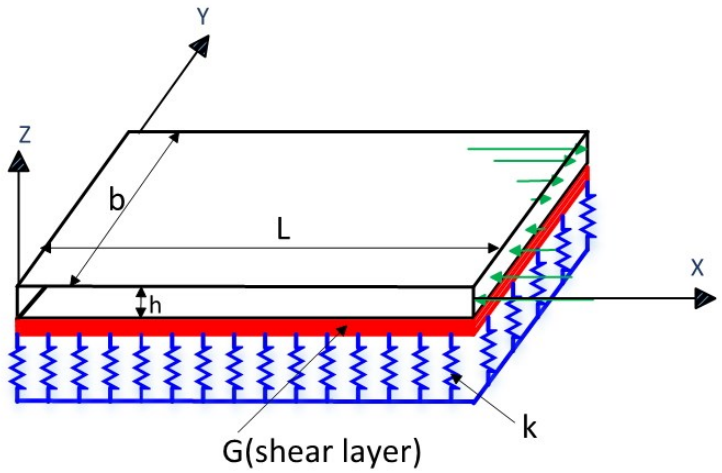

Figure 3.1. Orthotropic plate on Pasternak foundation under non-uniform in-plane load

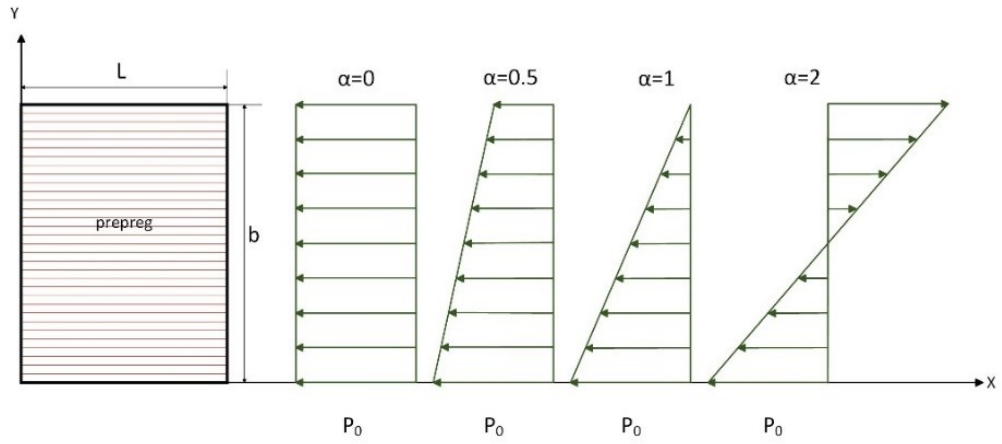

Figure 3.2. Different values of α and the resulting stress distribution

3.2.1 Rayleigh-Ritz Approach

The Rayleigh-Ritz energy approach is employed to determine the critical buckling load of this system. Compared to finite elements, this method has high degree of accuracy and computational efficiency [77]. The idea of this approach is to minimize the total energy $\Pi(w)$, which includes the elastic strain energy of the plate, potential energy of the foundation, and the potential energy of external work. The plate is considered to be thin and to undergo small deflections, satisfying Kirchhoff's hypothesis, where any normal to the plate mid-surface before deformation remains normal to the deformed mid-surface, and von Kármán approximations, where in-plane displacements are infinitesimal compared to the transverse deflection *w*.

$$\Pi(w) = U(w) + K(w) - Q(w) \tag{3.1}$$

The elastic strain energy of the plate is defined as [78]:

$$U(w) = \frac{1}{2}\int_0^b \int_0^L \left[D_{11}\left(\frac{\partial^2 w}{\partial x^2}\right)^2 + D_{22}\left(\frac{\partial^2 w}{\partial y^2}\right)^2 + 2D_{12}\frac{\partial^2 w}{\partial x^2}\frac{\partial^2 w}{\partial y^2} + 4D_{66}\left(\frac{\partial^2 w}{\partial x \partial y}\right)^2 \right] dxdy \tag{3.2}$$

D_{ij} is the bending stiffness of the plate and it can be defined as [79]:

$$D_{ij} = \int_{\frac{-h}{2}}^{\frac{h}{2}} Q_{ij}\, z^2 dz \tag{3.3}$$

Where

$$\begin{aligned} Q_{11} &= \frac{E_1}{1 - v_{12}v_{21}} \\ Q_{12} &= \frac{v_{21}E_2}{1 - v_{12}v_{21}} \\ Q_{22} &= \frac{E_2}{1 - v_{12}v_{21}} \\ Q_{66} &= G_{12} \end{aligned} \tag{3.4}$$

Then, the bending stiffness of an orthotropic plate can be given by

$$\begin{aligned} D_{11} &= \frac{E_1 h^3}{12(1 - v_{12}v_{21})} \\ D_{12} &= v_{21}D_{11} \\ D_{22} &= \frac{E_2}{E_1}D_{11} \\ D_{66} &= \frac{G_{12}h^3}{12} \end{aligned} \tag{3.5}$$

where E_1, E_2, v_{12}, v_{21}, and G_{12} are the elastic properties of the prepreg. The potential energy of the foundation that represents the prepreg tack and the shear layer is defined as [80]:

$$K(w) = \frac{1}{2}\int_0^b \int_0^L k.w^2 + G\left[\left(\frac{\partial w}{\partial x}\right)^2 + \left(\frac{\partial w}{\partial y}\right)^2\right] dxdy \tag{3.6}$$

where k and G are the normal and shear stiffness, respectively, related to the foundation and level of adhesion between prepreg and substrate. The potential energy of external work (in-plane stress) is defined as [78]:

$$Q(w) = \frac{1}{2}\int_0^b \int_0^L P\left(\frac{\partial w}{\partial x}\right)^2 dxdy \tag{3.7}$$

where P is the distributed load applied by steering at the side edges. Load through the tow width can be expressed as [81]:

$$P = P_0\left(1 - \frac{\alpha y}{b}\right) \tag{3.8}$$

where P_0 is the maximum compressive load applied at the inner edge of the plate.

The deflection shape w is assumed based on the selected boundary conditions and the applied load. It has also to be appropriate for a closed-form solution using the Ritz method, and it is defined as:

$$w = \sum_{i=1}^{n} a_i\left(1 - \frac{y}{b}\right)^{i+1}\left(1 - cos\frac{2\pi mx}{L}\right) \tag{3.9}$$

The critical buckling load is obtained by considering only one term of the deflection as equation (3.9) and substituting it into equations (3.2), (3.6), and (3.7), the final derivation of these three equations is given as:

$$\mathrm{U} = a_1^2\left[\frac{4}{5}D_{11}bL\left(\frac{\pi m}{L}\right)^4 + \frac{(16D_{66}-4D_{12})L}{3b}\left(\frac{\pi m}{L}\right)^2 + \frac{3D_{22}L}{b^3}\right] \tag{3.10}$$

$$\mathrm{K} = a_1^2\left[\frac{3}{20}kbL + \frac{1}{5}GbL\left(\frac{\pi m}{L}\right)^2 + \frac{GL}{b}\right] \tag{3.11}$$

$$\mathrm{Q} = a_1^2(6-\alpha)\left(\frac{\pi m}{L}\right)^2\left(\frac{bL}{30}\right)P \tag{3.12}$$

These equations are then substituted into equation (3.1) and differentiated with respect to the amplitude (a). The resulting critical buckling load is given by:

$$P_{cr} = \frac{1}{6-\alpha}\left[\begin{array}{c}24D_{11}\left(\frac{\pi m}{L}\right)^2 + 160D_{66}\frac{1}{b^2} - 40D_{12}\frac{1}{b^2} + 90D_{22}\left(\frac{L}{\pi m b^2}\right)^2 \\ + \frac{9}{2}k\left(\frac{L}{\pi m}\right)^2 + G\left(30\left(\frac{L}{\pi m b}\right)^2 + 6\right)\end{array}\right] \tag{3.13}$$

where *m* is the number of waves in a buckling mode, which assumed to equal to one as only one isolated wrinkle is considered in this model.

3.2.2 Steering Radius

When the prepreg tape is steered, the length of the required path does not match the length of the unidirectional fibers at the inner and outer edge of the tape. This unbalanced length generates a constant in-plane load that can be derived from the geometrical shape of the steered tape, assuming the tape is steered at radius R and angle θ, as illustrated in Figure 3.3. The length of the tape L is equal to ($R\theta$) at the neutral access, which depends on the stress distribution factor α. For instance,

the neutral access is at the middle when α equals 2. The length of the inner edge of the steered tape is $\theta(R - b/\alpha)$, therefore, the strain caused by the difference of length can be written as $b / (R\alpha)$. As a result, the maximum steering load applied at the inner edge of the tape can be derived by the stress-strain relationship and is given as:

$$P_0 = \frac{E_1 hb}{R\alpha} \tag{3.14}$$

where R is the steering radius, b and h are the width and the thickness of the tape, respectively, and E_1 is the young's modulus of the tape.

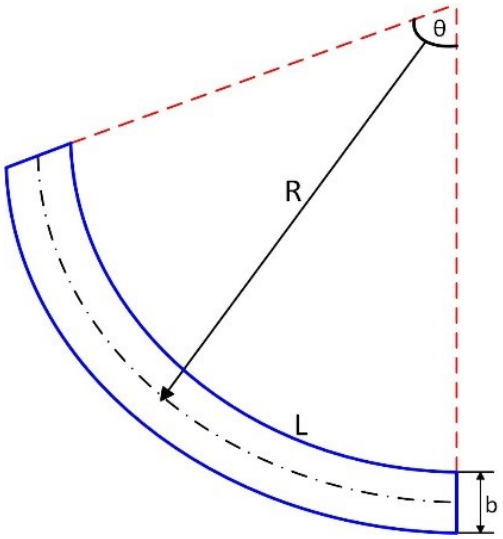

Figure 3.3. Representation of a steered tape

The critical steering radius is found by using steering load (equation (3.14)) and critical load (equation (3.13)). When the steering load applied on the tape is more than the critical load, buckling will occur. If the steering load is less than the critical load, then no buckling will be achieved. At the point when the steering load (equation (3.14)) is equivalent to the critical load (equation (3.13)) relating to the limit among buckling and no buckling, this case is used to define

the critical steering radius. The minimum load, as shown in equation (3.15), is obtained by differentiating critical load (equation (3.13)) with respect to wavelength L. The detailed derivations are presented in Appendix A. Then, the critical steering radius is found by solving the minimum load (equation (3.15)) with the steering load (equation (3.14)). The minimum load and the critical steering radius are found to be:

$$P_{min} = \frac{2}{6-\alpha}\left[\frac{360\sqrt{3}D_{22}D_{11} + 18\sqrt{3}kb^4D_{11} + 120\sqrt{3}Gb^2D_{11} + 2I(40D_{66} - 10D_{12}) + 3Gb^2I}{b^2I}\right] \quad (3.15)$$

$$R_{cr} = \frac{(6-\alpha)Ehb^3I}{2\alpha\left[360\sqrt{3}D_{22}D_{11} + 18\sqrt{3}kb^4D_{11} + 120\sqrt{3}Gb^2D_{11} + 2I(40D_{66} - 10D_{12}) + 3Gb^2I\right]} \quad (3.16)$$

where

$$I = \sqrt{D_{11}(180D_{22} + 9kb^4 + 60Gb^2)} \quad (3.17)$$

3.2.3 Wrinkle Wavelength

When the steering load (equation (3.14)) is greater than the critical load (equation (3.13)), wrinkles occur, and the length of these wrinkles can be determined by solving these two equations. The detailed derivations are presented in Appendix A. The wrinkle wavelength can be found by solving the biquadratic equation (3.18). This equation gives real solution only with steering radii less than the critical radius. While the solution is only complex roots if the steering radius is greater than the critical radius in which no wrinkles take place.

$$AL^4 + BL^2 + C = 0 \quad (3.18)$$

With:

$$A = 90D_{22}\left(\frac{1}{\pi mb^2}\right)^2 + \frac{9}{2}k\left(\frac{1}{\pi m}\right)^2 + 30G\left(\frac{1}{\pi mb}\right)^2 \quad (3.19)$$

$$B = 160D_{66}\left(\frac{1}{b^2}\right) - 40D_{12}\left(\frac{1}{b^2}\right) - (6-\alpha)\left(\frac{Ehb}{\alpha R}\right) + 6G \tag{3.20}$$

$$C = 24D_{11}(\pi m)^2 \tag{3.21}$$

3.3 Model Parameters Determination

3.3.1 Elastic Modulus (E_1)

The properties of the uncured prepreg are not available in the material data sheet. Thus, some properties were experimentally characterized. The longitudinal elastic modulus was obtained by a tensile test. The tow sample was cut with an 80 mm length and kept at room temperature for 30 min before it was gripped at two ends by the apparatus. The applied tensile load was recorded as a function of displacement as shown in Figure 3.4. This curve was converted to a stress–strain curve and the material elastic modulus was extracted as the slope of this curve as shown in Figure 3.5. Note that the presented curve is the average of three test trials.

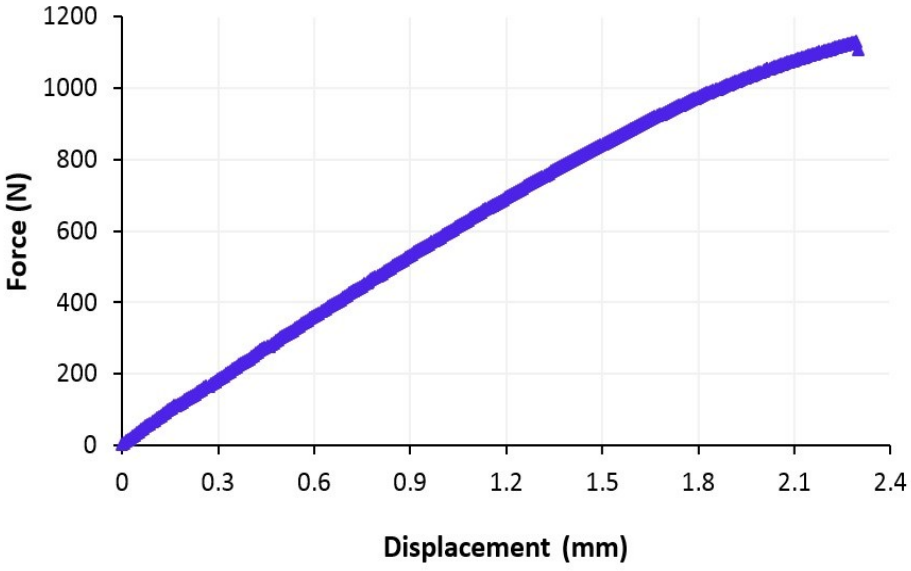

Figure 3.4. Uniaxial tensile test response of prepreg tow

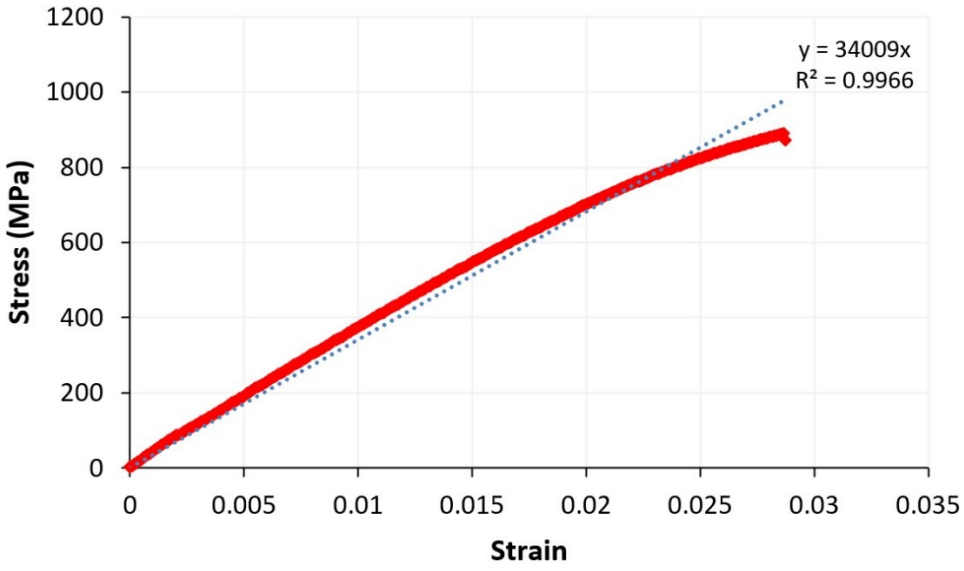

Figure 3.5. Stress vs. strain curve used to determine the value of elastic modulus

3.3.2 Normal Stiffness of Foundation (*k*)

Normal stiffness represents the material tack which is defined as the energy required to detach two surfaces placed in contact for a short time under light pressure [62]. In this study, a simple probe tack test was used to measure the normal stiffness using a tensile machine. The lower grip of this machine was replaced by a support to hold the prepreg sample during the test. The aluminum probe was mounted in the upper grip of the machine, as shown in Figure 3.6 (a). The prepreg sample was cut and kept at room temperature for 30 min, then it was placed on the support without any pressure. The processing temperature chosen for this test was 45 °C, which represents the material temperature during AFP process. When the test started, the probe came into contact with the sample for 60 sec at 10 N contact force before it was debonded at a crosshead rate of 100 mm/min. The force required for debonding was recorded as a function of displacement as shown in Figure 3.6 (b). It should be noted that only the recorded force and displacement values during the removal phase (before the maximum debonding force) were used in this section. Then it was converted to

stress vs. displacement curve by applying the section area of the probe. The average of the debonding force-displacement curves, presented in Figure 3.6 (b), was used to plot Figure 3.7. A linear fit was applied to the stress versus displacement curve (Figure 3.7) and the normal stiffness value *k* is given by the slope of this linear trend.

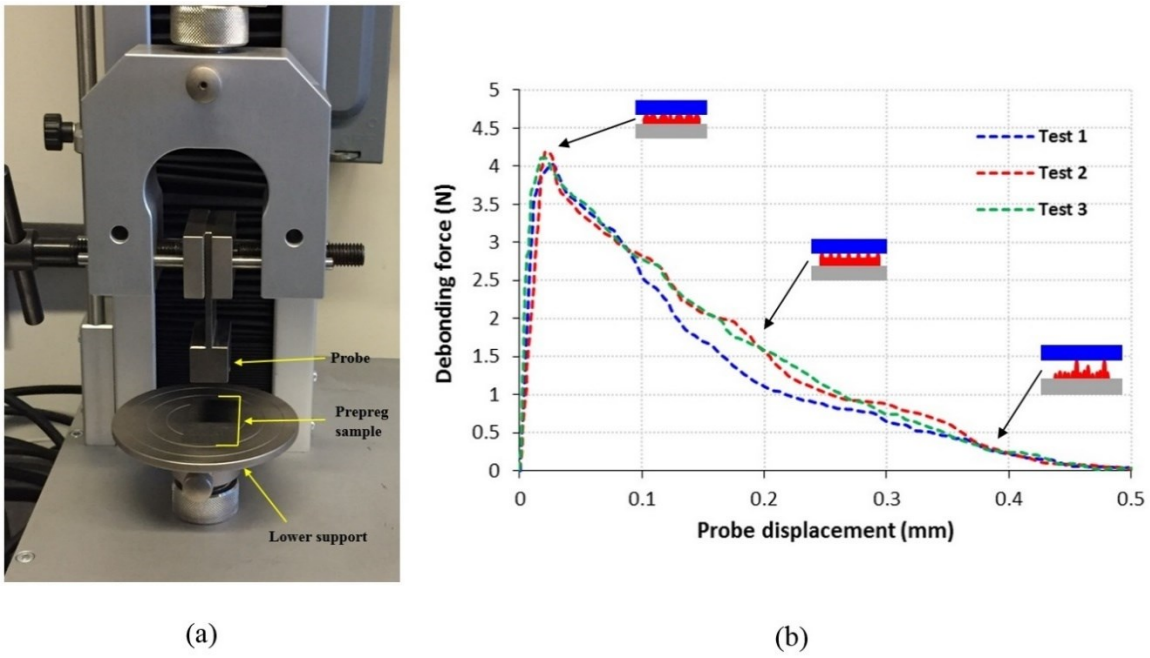

(a) (b)

Figure 3.6. (a) Test machine; (b) debonding force vs. probe displacement curve indicating the debonding stages throughout the test

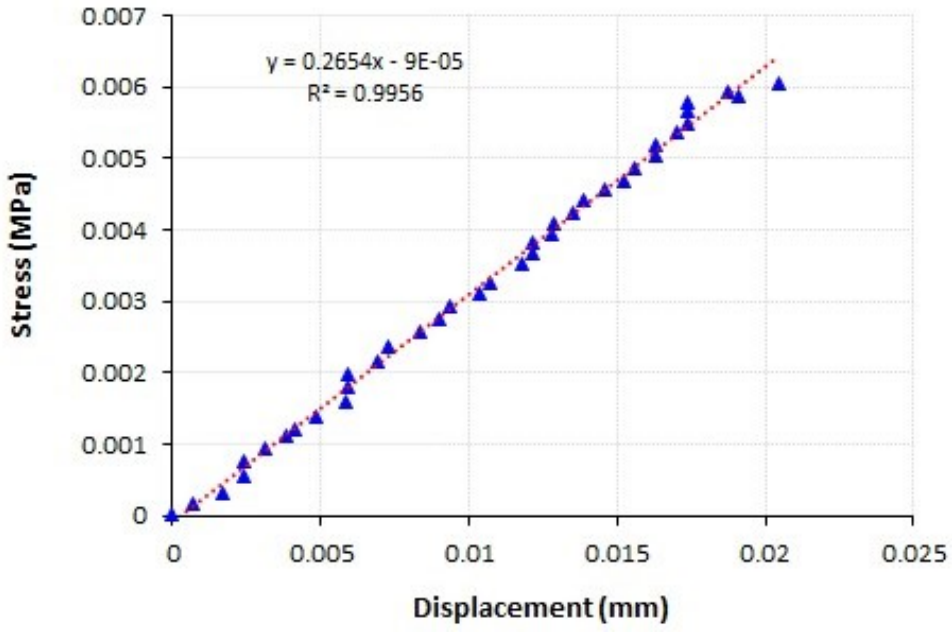

Figure 3.7. Stress-probe displacement curve of removal phase with linear fit for prepreg sample

3.3.3 Shear Stiffness (*G*)

Although the shear stiffness (*G*) is related to the shear layer corresponding to the foundation and adhesion, it is difficult to obtain it through characterization method. Therefore, the shear stiffness of the shear layer was assumed to be equal to the shear stiffness of the prepreg. A bias extension test was used to determine the shear modulus of the uncured prepreg. In the bias extension test, the material is extended along the bias beginning at ±45º to the direction of the applied tensile force. The specimens selected for the bias extension test were 120 mm long by 40 mm wide, with an ungripped length of 80 mm. Each sample was made of two ±45° layers that were pre-consolidated at 70 °C with 0.1 MPa (vacuum pressure) for 30 minutes.

The tests were performed using a tensile testing machine and non-contacted infrared lamps. The processing temperature chosen for this test was 45 °C with a crosshead rate of 100 mm/min. The specimen for the test can be divided into three zones, as depicted in Figure 3.8 (a). In order to

obtain a uniform deformation in zone A, the specimen's length L must be equal to or greater than twice its width W [77, 78]. A total of three trials were performed to ensure accuracy and experiment repeatability.

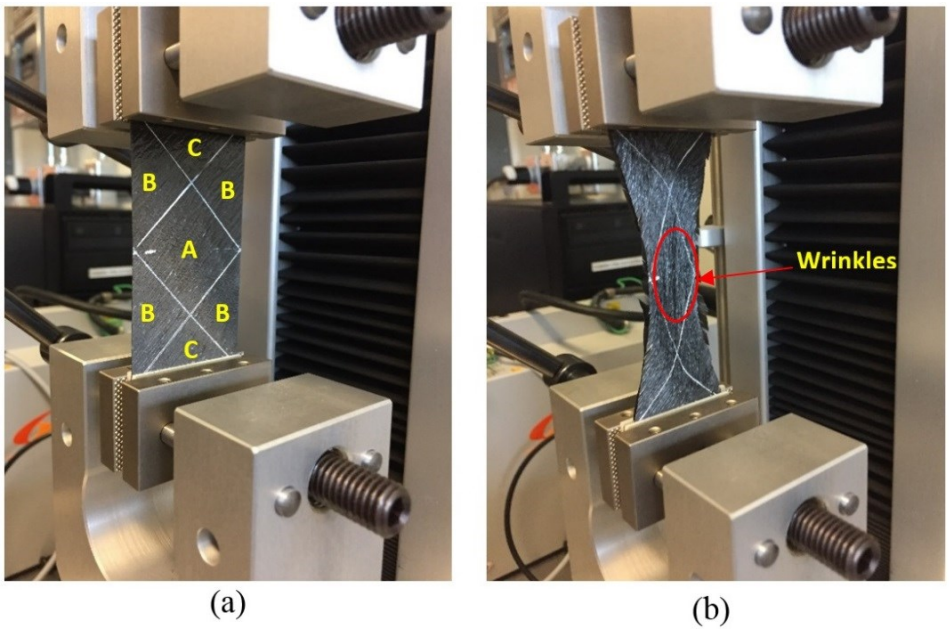

Figure 3.8. (a) Undeformed sample; (b) Deformed sample

The force and displacement were recorded as shown in Figure 3.9. The force was converted to the normalized shear stress using equation (3.22) [84]. The shear angle throughout the test was captured by a digital camera, and the images were inserted into software to measure the corresponding angles. The shear stiffness was calculated based on the normalized shear stress and the resulting shear angle (radian). During the test, some wrinkles appeared on the sample at a specific time, as shown in Figure 3.8 (b). To avoid the effect of these wrinkles on the results, the captured images were used to determine the time of wrinkling onset. Accordingly, the data used to calculate the shear stiffness of the prepreg were selected before this time.

$$\sigma_{norm} = \frac{Fsin45}{tWsin\gamma} \tag{3.22}$$

where σ_{norm} is the normalized shear stress of bias extension test, F is the force, t and W are the thickness and the initial width of the specimen, respectively, and θ is the shear angle.

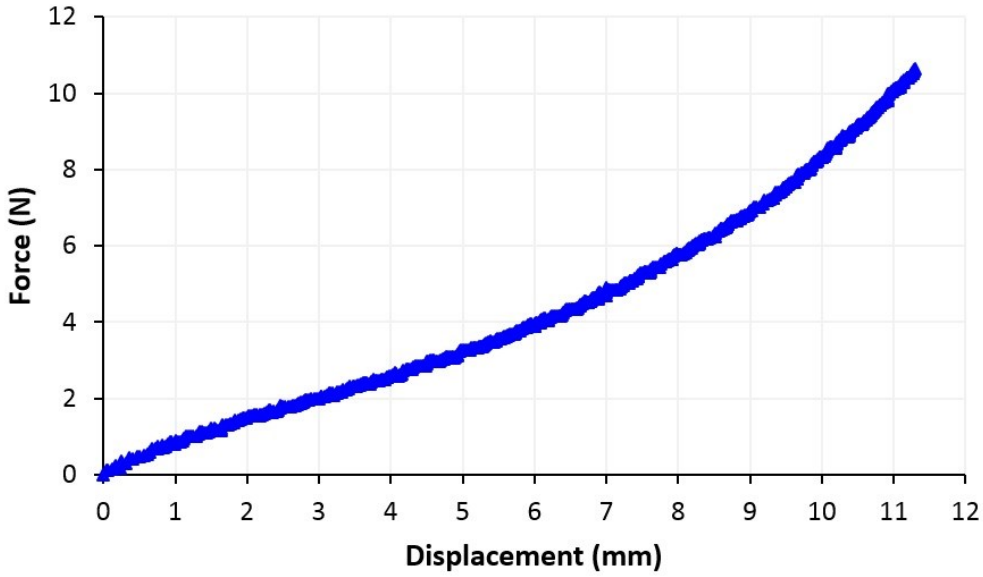

Figure 3.9. Force vs. displacement curve recorded during bias extension test

In order to determine the material shear stiffness *G*, the normalized shear stress was calculated based on the applied shear force. The wrinkles generated during the test, shown in Figure 3.8 (b), were considered for the determination of the shear stiffness; only the initial part of the curve, prior to wrinkling onset, was used. Figure 3.10 shows the normalized shear stress against the captured shear angle (rad) plot, which indicates the regions before and after the wrinkling initiation. The shear stiffness was obtained as the slope of the linear trend of this curve. The elastic properties of the prepreg used in the calculation and the required parameters for the critical radius (equation (3.16)) are presented in Table 3.1.

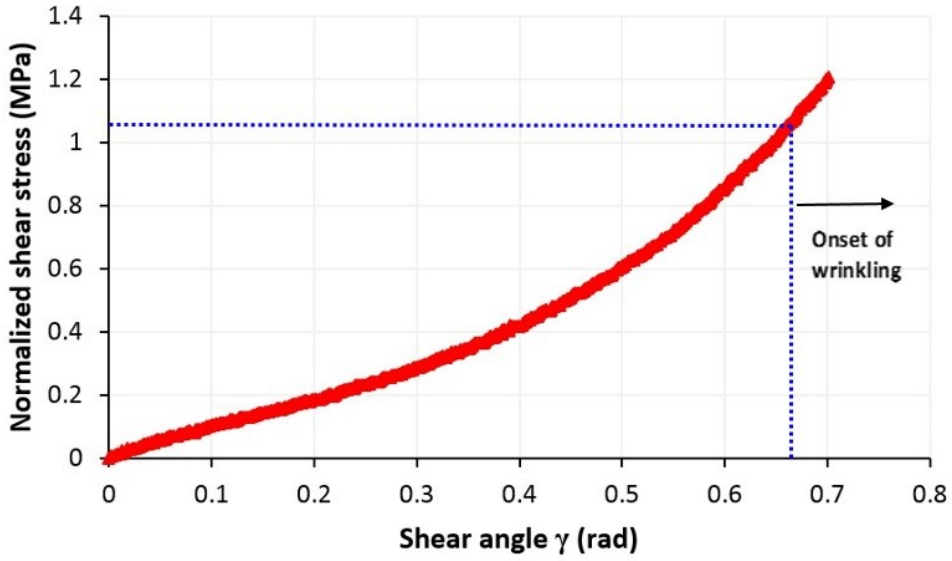

Figure 3.10. Normalized shear stress plotted against shear angle. The dotted line indicates the region used for the calculation

Table 3.1. Elastic properties of the prepreg and required model parameters

Parameter	E_1 (GPa)	E_2 (MPa) [53]	ν_{12} [54]	ν_{21} [54]	α	h (mm)	b (mm)	k (N/m^3)	G (N/m)
Value	34	0.046	0.2	0.02	2	0.2	6.35	2.65×10^8	605

3.4 Experimental Verification

The AFP machine used for performing this experimental work was an XTP-500 supplied by Automated Dynamics and is depicted in Figure 3.11 (a). This machine has six degrees of freedom. It can lay-up both thermoplastic and thermoset composites by changing the placement head. The placement head for the thermoset material used in this work has the ability to adjust up to 4 tows, with individual tow widths of 0.25 in (6.35 mm). The material used in this process is available in two forms, prepreg tow and slit tape. Both forms are wound onto cardboard bobbins (spools).

During the automated lay-up process, based on the size and the shape of the manufactured part, a number of prepreg spools are loaded into the machine system. The individual tows can be started and cut at any time during the process in order to increase or decrease the width of the tow band. The tows are fed onto the surface by a compaction roller and heated by a heat source such as a hot gas torch or laser. A schematic of the fiber placement process is illustrated in Figure 3.11 (b). When the thermoset tape is used, the applied heat makes the material tackier and ensures that it will stick onto the mold after the compaction roller passage. When the first band is completed, all tows are cut, and a new band is started until the required number of plies is accomplished.

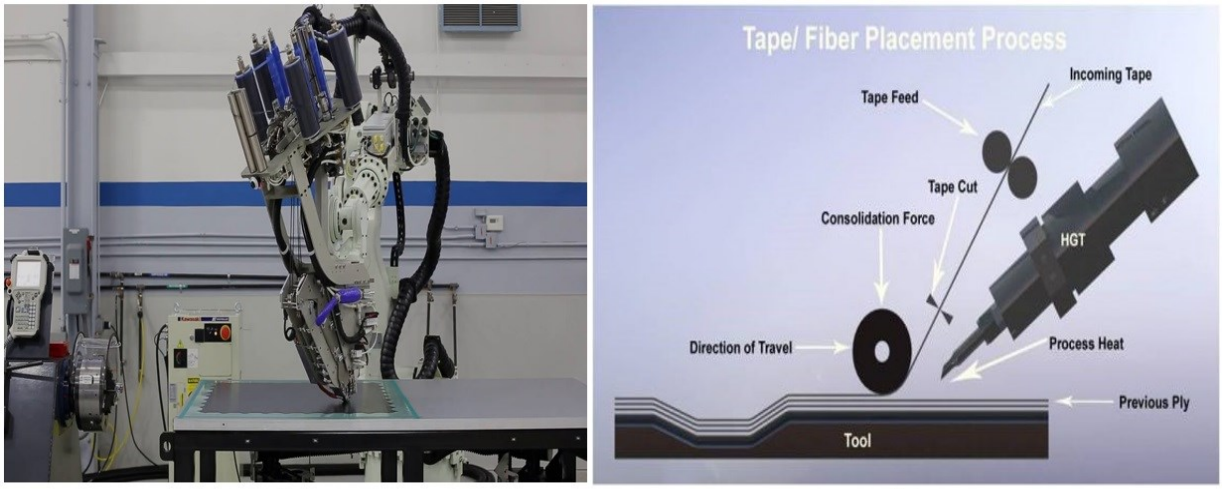

(a) (b)

Figure 3.11. (a) AFP machine from Automated Dynamics; (b) schematic of AFP system [5]

The material used for the steering trials was a ¼ in unidirectional prepreg (CYCOM 977-2/ HTS-145). This material consists of an HTS-145 high-strength grade 12K carbon fibers impregnated with CYCOM 977-2 (177°C) curing epoxy resin system, which is manufactured for autoclave or press molding, and is recommended for the production of large structures [85]. This material system has a 60% fiber volume and a thickness of 0.2 mm. The purpose of this experimental work is to validate the theoretical model in terms of critical steering radius and the

wrinkle wavelength. To get the experimental results, two different procedures were performed. First, multiple-different radii were chosen to be steered at the same process parameters reported in Table 3.2. These parameters were set in the machine system while the tool temperature was manually measured using a thermocouple. Before the lay-up process, the material was kept at room temperature for 30 minutes. Then, it was directly steered on an aluminum tool, as illustrated in Figure 3.12 (a). This tool was cleaned after each trial using acetone to ensure that there was no residual resin on the surface that might affect the results. The wrinkle wavelength was measured manually. First, the tapes were laid-up with different steering radii in which wrinkles were clear to be measured. Second, an adhesive tape was used to facilitate counting the wrinkles along each steered tape, as shown in Figure 3.12 (b). Finally, the average wavelength was calculated for each steering radius as the length of the prepreg tape divided by the number of the formed wrinkles.

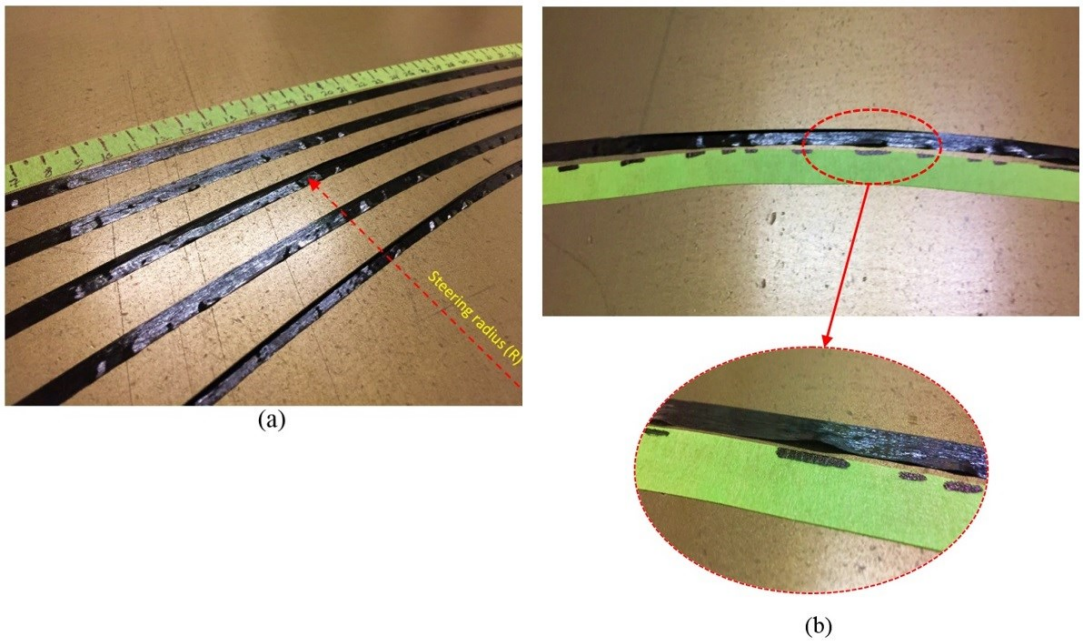

Figure 3.12. (a) Steered tows on Aluminum tool; (b) wavelength measurement using adhesive tape

Table 3.2. Process parameters used in the steering trials

Parameter	Lay-up speed (in/sec)	Compaction force (lb)	Torch temperature (C^o)	Tool temperature (C^o)
Value	3	60	130	23

3.5 Critical Steering Radius

The critical steering radius results based on equation (3.16) are compared to the experimental observations at different radii. Figure 3.13 (a) shows a set of tows steered with the same process parameters (Table. 3.2) at different steering radii ranging from 60 cm to 180 cm. Three trials were steered for each radius to check the repeatability of the process. No clear difference among the three trials was observed; therefore, only the last trial was used to present the results. The steered tows were individually observed to check the occurrence of out-of-plane wrinkling. The results show that the wrinkling is clear on the tows steered with a radius up to 80 cm. It should be noted that bridging was more dominant than wrinkling within these tows because the radius is too small to be steered. The out-of-plane wrinkling gradually decreased with increasing the steering radius until they totally disappeared above the steering radius of 120 cm. Consequently, this steering radius can be considered the critical radius measured during the process. Figure 3.13 (b) illustrates the wrinkles on three different tows selected from the ones shown in Figure 3.13 (a). This figure shows how wrinkles decrease as the steering radius goes higher before they vanish at the critical radius (120 cm). However, in-plane waviness was observed in each of the steered tows, as shown in Figure 3.14. In-plane waviness is an inherent lay-up defect of steering that occurs prior to out-of-plane buckling [74].

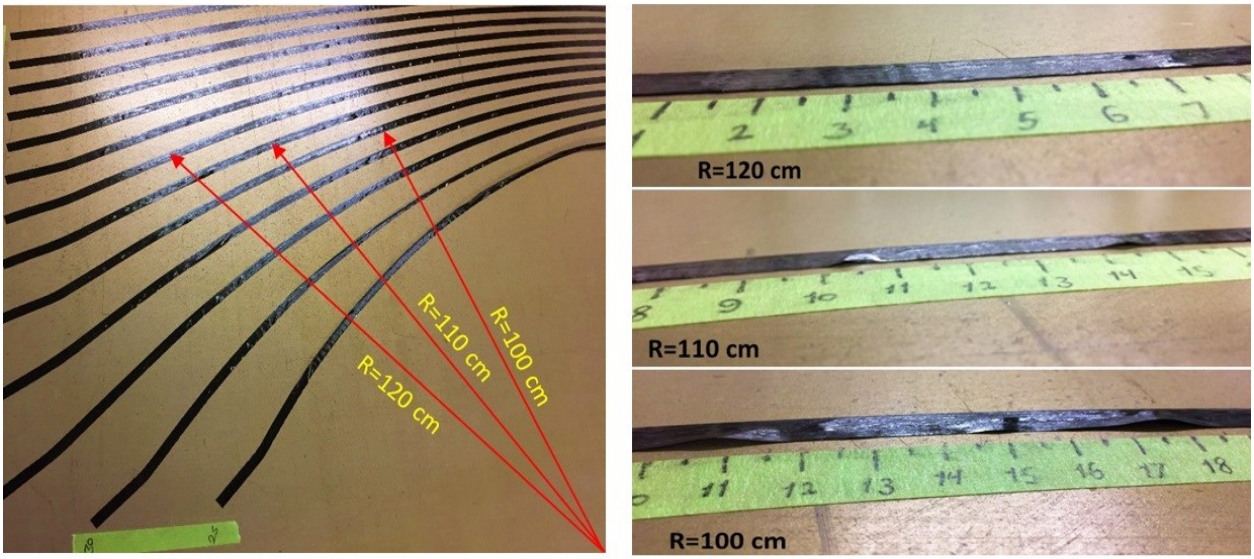

Figure 3.13. (a) Steered tows on aluminum tool for out-of-plane wrinkling observation; (b) three tows steered at different radii (100, 110, and 120 cm)

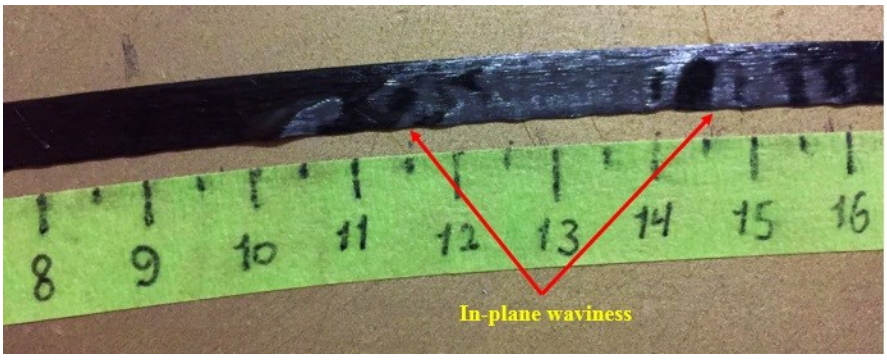

Figure 3.14. In-plane waviness as a steering defect on a steered tow

Theoretically, the model parameters listed in Table. 3.2 were used to calculate the critical steering radius (equation 3.16). The results show that the selected material can be steered up to 136 cm as a critical radius without out-of-plane buckling. This predicted critical radius was too close to the measured one (120 cm), which demonstrates the capability of this model to predict the

critical steering radius. The resulting critical radius without considering the shear layer (G) [54] was found to be 170 cm. This confirms that the developed model presented in this work increases the design flexibility by lowering the steering radii. However these steering radius values can be significantly affected by changing the process parameters such as lay-up speed and temperature [86], where shear layer can be used to capture some of those effects. This effect is also attributed to the viscoelastic behavior of the resin.

Figure 3.15 represents the critical steering radius of the prepreg tow as given by equation (3.16) against the normal stiffness (k), the other used parameters used in the equation are presented in Table 3.1. The curve shows that the critical steering radius is highly influenced by the normal stiffness, which represents the tack of the prepreg. The critical steering radius is decreased from 1.8 m to 0.8 m when the normal stiffness of the foundation increases from 1×10^8 N/m^3 to 1×10^9 N/m^3. This describes the importance of the tackiness effect on wrinkle formation. The tackiness properties can be improved by increasing the temperature and decreasing the lay-up speed and hence, increasing the lay-up quality [67]. Therefore, k has to be characterized based on the processing and manufacturing conditions.

The critical steering radius of the prepreg tow as given by equation (3.16) is plotted against the stress distribution factor (α) in Figure 3.16. The stress distribution factor α accounts for the additional stresses such as the tension in the tow to the in-plane bending generated by steering. The critical radius was calculated using the parameters mentioned in Table 3.2 with varying values of α selected between 1 and 2. The range of α was selected according to Beakou et al. [53]. The graph also shows that a smaller critical steering radius can be achieved by increasing the value of α. However, when the value of α exceeds two, the outer edge of the tow will be stretched and causes bridging.

Figure 3.17 illustrates the critical steering radius of the prepreg tow as given by equation (3.16) versus the shear stiffness of the foundation (G). The results show that increasing the shear stiffness of the shear layer reduces the critical steering radius. As the shear stiffness increased from 0 to 1000 N/m, the critical steering radius decreased by approximately 30%. In order to minimize the critical steering radius, shear stiffness should be increased. However, the shear stiffness decreases by increasing the temperature, unlike the normal stiffness (k). This may indicate that higher temperature during automated lay-up is not always recommended. Shear stiffness of the shear layer is related to the tackiness and adhesion of the prepreg to the substrate. It is a function of processing conditions and has to be characterized.

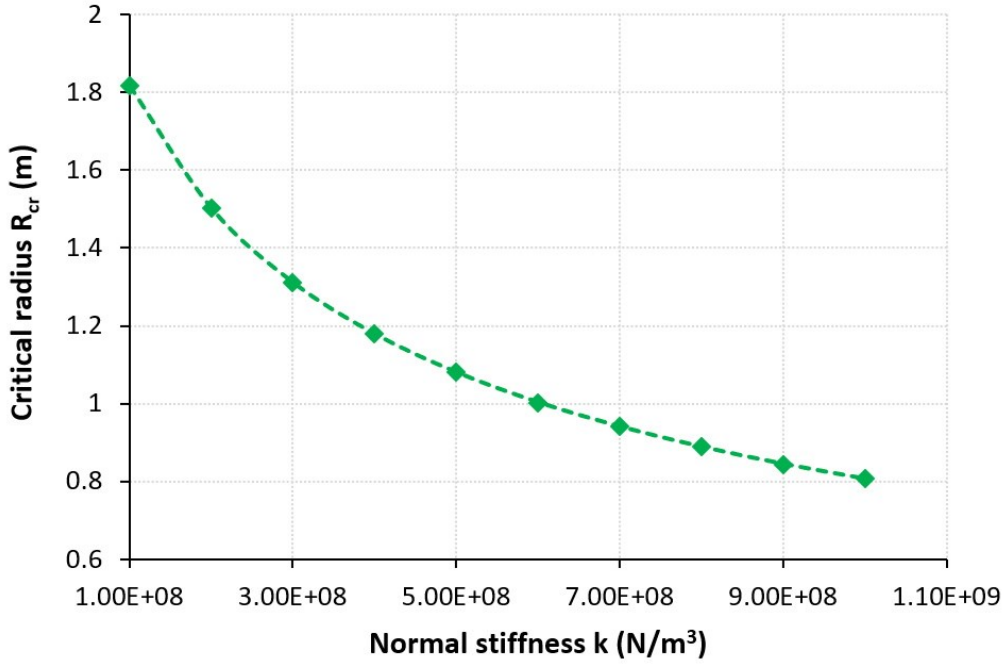

Figure 3.15. The critical steering radius of the prepreg tow plotted against the normal stiffness of the foundation (k)

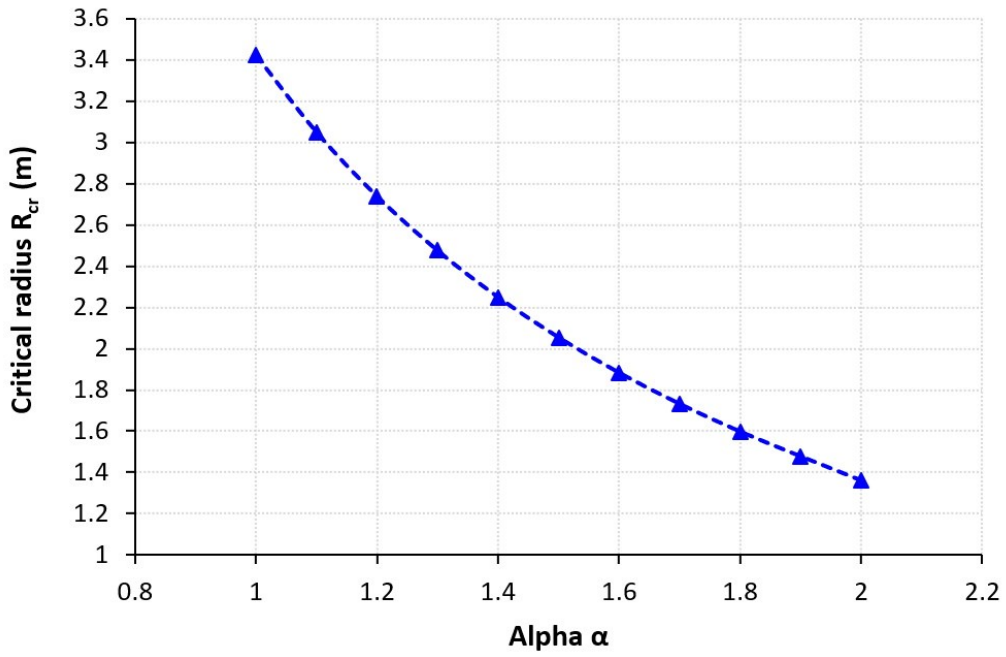

Figure 3.16. The critical steering radius of the prepreg tow plotted against the stress distribution factor (α)

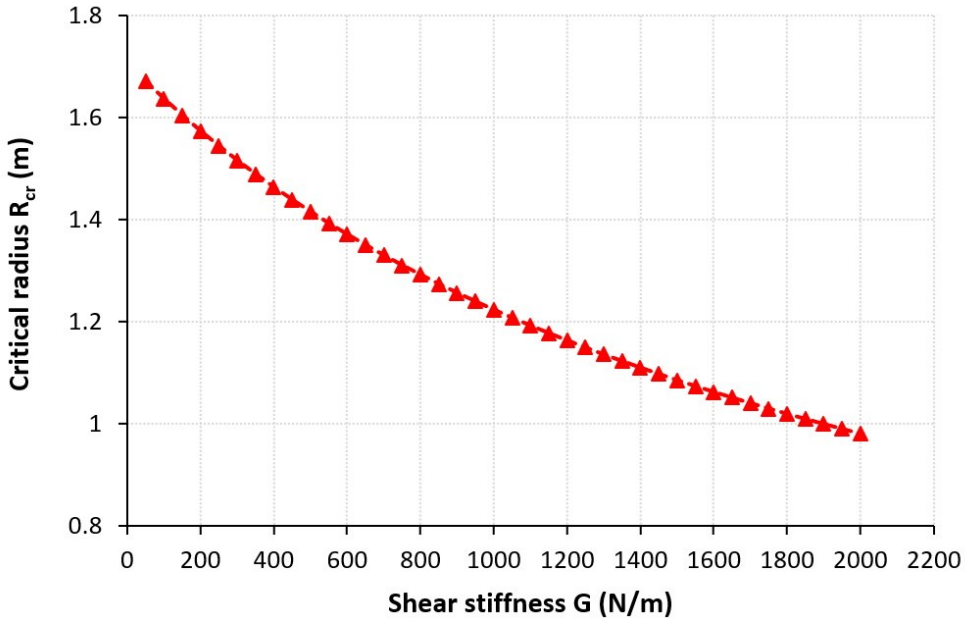

Figure 3.17. The critical steering radius of the prepreg tow plotted against the shear stiffness of the foundation (*G*)

3.6 Wrinkle Wavelength

The wrinkle wavelength (equation 3.15) was calculated for various values of steering radius smaller than the critical steering radius determined in the previous section. The same values of steering radii used to calculate the wavelength were experimentally steered to measure the average wavelength for each radius. Both calculated and measured wavelengths are plotted against the steering radius in Figure 3.18. The results show good agreement between the calculated and measured wavelengths. All the experimental values were slightly larger than their counterparts obtained by the model except one, which was smaller but closer to the calculated value. In addition, the buckling wavelength increases by increasing the critical radius till the wavelength becomes infinite (complex numbers) when it reaches the critical radius, which means there is no buckling. This equation can be used to predict length of buckling to confirm a high quality of the lay-up.

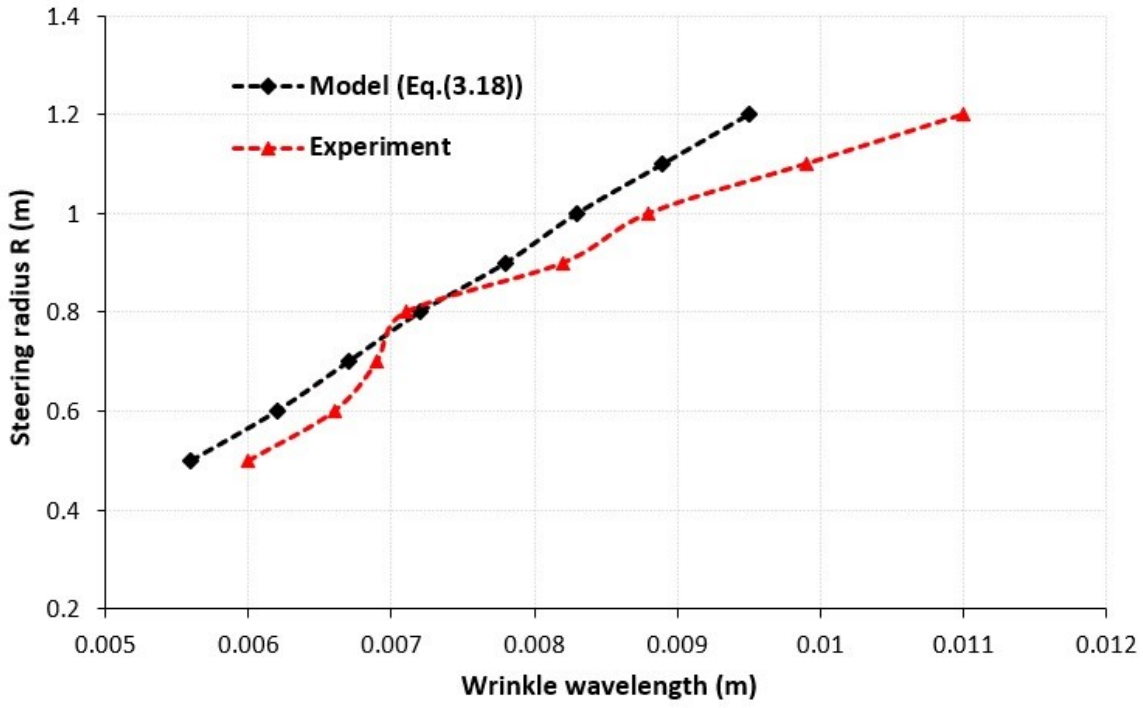

Figure 3.18. Steering radius vs. wrinkle wavelength

3.6 Summary

A theoretical model based on the Rayleigh-Ritz approach was presented to study wrinkle formation during steering of thermosetting composite prepreg using an AFP machine. A Pasternak elastic foundation with a shear layer was used to present the elastic foundation. This model has the capability to predict the critical steering radius at which no wrinkles will occur. It can also predict the buckling wavelength at steering radii smaller than the critical radius. The calculated critical steering radius and buckling wavelength based on the model were validated with a set of experimental trials. The predicted values were found to be in good agreement with the experimental values. However, there was an inconsiderable difference between the model and the experimental results due to the effect of process parameters. When this model is compared to the same model without a shear layer, there was an important difference in terms of critical steering radius. This explains the significance of the foundation shear layer represented in the model by the shear stiffness. During the experimental work, it was found that process temperature and lay-up speed strongly influence the wrinkle formation and, hence, the critical steering radius because of their effect on the viscoelastic behaviour of the prepreg and its adhesion to the substrate.

Chapter 4: Experimental investigation of prepreg tack

4.1 Introduction

Advanced composite materials are increasingly being used in areas of industry where strength and stiffness-to-weight ratios are essential factors. Automated tape laying (ATL) was introduced in the 1970s as the automated alternative of the traditional hand layup. It has been used to produce large simple structures with high quality and low cost. For more complex structures, automated fiber placement (AFP) was adopted later in the 1980s, particularly in the aerospace industry. This technology can accommodate up to 32 tows; each tow (3.175–6.35 mm) can be cut and restarted individually during the layup process [8]. In AFP, a robotic fiber placement head uses a predefined path to apply the prepreg on the mold surface. The adhesion level between the applied prepreg and the surface of the mold or between the adjacent layers of the prepreg plays an essential role in the quality of the produced part. Most defects generated during the layup process, such as wrinkling and tow pull-up, are related to the poor tack level, which cannot resist the detaching interface forces [53].

Several studies have analyzed prepreg tack characterization using different approaches and different methods [65, 82-84]. Tack is one of the crucial properties that dominate the layup process and, hence, quality of the final product. To accomplish a high tack level, the influence of some process parameters such as temperature, speed, and compaction force on this property is being investigated. Bakhshi and Hojjati [85, 86], for example, studied the effect of compaction force and different types of rollers on the defect formation. The authors observed changes in defect size and distribution by using different rollers. It was reported that the roller made of solid elastomer presents a layup with lower defects. The authors also introduced a probe FEM simulation that

predicts wrinkle and blister formation. Belhaj and Hojjati [56] studied the effect of steering on wrinkle formation during the AFP process. They presented a model to predict the optimum value of steering radius that can be laid-up without wrinkle formation. They used a simple probe test to characterize the prepreg tack at the same AFP process parameters.

Dubois et al. [62] used the same test to characterize the tackiness of prepreg considering the maximum debonding force as a measurement of the tack level. They performed the test on pure resin and prepreg. For the prepreg, the results show that increasing temperature decreases resin viscosity and reduces the resin content at the prepreg–probe contact area. Consequently, it decreases tackiness on the probe side and increases it on the other side. The authors also concluded that increasing the debonding rate will increase the maximum debonding force. Moreover, they found this test to be sensitive to changes in surface roughness led by fiber pattern and resin distribution within the sample. A probe test is a precise method to provide bonding and debonding rates. However, the applied load varies from that in the AFP process. Furthermore, this test can only measure a limited area of the prepreg in each run, which does not take into consideration the prepreg homogeneity.

Budelmann et al. [92] investigated the prepreg tack behavior at different process and material parameters using a probe tack test executed by a rheometer. The authors found that prepreg tack is highly affected by temperature variation. Maximum tack was reported at higher temperatures. Regarding the compaction force effect, the authors stated that increasing compaction force consistently improves prepreg tack up to a specific compaction force level. Exceeding this level demonstrated minor effect on prepreg tack. However, the results of this test can be improved by testing samples made by the real AFP process. Moreover, using a rheometer as a measuring tool limits the results for only a small piece of the processed material. Wohl et al. [64] also used a

rheometer to determine prepreg tack by probe test. The tests were carried out on a stainless-steel probe at different environmental conditions, including temperature and humidity. The authors pointed out that increasing humidity improves tackiness, while increasing temperature and debonding rate slightly influences the tack strength. They added that applying more than a threshold contact force value decreases or has no effect on prepreg tack.

Crossley et al. [66, 69] designed a test setup that imitates the automated layup process to characterize both tack and dynamic stiffness of uncured prepreg. They found a correlation between failure mode and temperature. In the dry failure mode, increasing the temperature causes higher tackiness; in the wet failure mode, increasing the temperature has a reverse effect. The authors also reported nonlinear behavior of the prepreg tack as a function of layup temperature and speed of deformation. Endruweit et al. [69] used the same test apparatus (continuous application-and-peel test method) to characterize the prepreg tack with more focus on the surface combination and prepreg conditions. The authors indicated that the tackiness of the prepreg surface covered with the backing paper was higher than the other side of prepreg. Rao et al. [65] investigated the influence of compaction load, layup speed, and temperature on the tackiness properties of AFP grade prepreg. The layup process was simulated on a CNC milling machine, while a floating roller peel test was used to investigate the adhesion properties of the prepreg. The authors stated that, at high feed rates, higher temperatures are required to have good influence on prepreg tack. Also, they reported a different temperature effect at low and high compaction loads. They concluded that interaction between different process parameters could be another factor behind the obtained results. Thus, the effect of process parameters should be synergistically investigated.

In this chapter, we aim to investigate the influence of layup process parameters, including temperature, compaction force, feed rate, and placing a roller on a carbon-fiber epoxy/prepreg

tack. Two different setups are employed; the first setup simulates the AFP process with the ability to adjust all mentioned process parameters; the second performs a 90º peel test to measure the prepreg tack as the average peel force. The Taguchi method is implemented on the obtained results to optimize the layup process parameters and to find the optimal combination for high layup performance. First, this method is used to optimize the process parameters, including heat gun temperature, compaction force, and feed rate. Second, it is used to study the effect of using different rollers to find the best roller. The purpose is to demonstrate a better understanding of tack phenomena and to find the best process parameters for optimizing the layup process.

4.2 Layup Process Setup

An in-house fiber placement setup was designed and built to simulate the AFP process and control the process parameters. As shown in Figure 4.1, in this setup, a pneumatic air pressure cylinder connected to a load cell is used to control and read the compaction force. The air jack is connected to a steel bracket, which holds the compaction roller. The roller is made from polyurethane and has the same dimensions as the original AFP roller [90]. To perform the layup movement with a fixed placing roller, a ball screw linear guide is used to move the mold during the layup at the required speed. This linear guide has a traveling distance of 60 cm and an adjustable speed varying from 1 to 125 mm/sec. For the heating, a heat gun is mounted and directed toward the NIP point with a 15° angle and 100 mm from the heated area. An infrared thermal camera is used to monitor the mold and material temperature throughout all layup process. The mold used to place the prepreg on is a 300 mm long removable aluminum plate, which can be easily transferred to the peel test setup.

The material system used here is a 6.35 mm (1/4 in) 977-2/35-12K HTS-145 unidirectional prepreg. To adjust the prepreg tension, the spool holder is connected to a clutch where the tension is simply controlled. A plastic guide is used to guide the prepreg from the spool to the mold surface and provide the required layup position. Before the layup process, the material was kept at room temperature for at least six hours, and the aluminum plates were cleaned with acetone. All the process parameters and rollers were changed based on the test requirements, which will be explained in the results and discussion section. Three samples are laid-up for each test and transferred immediately to the peel test setup.

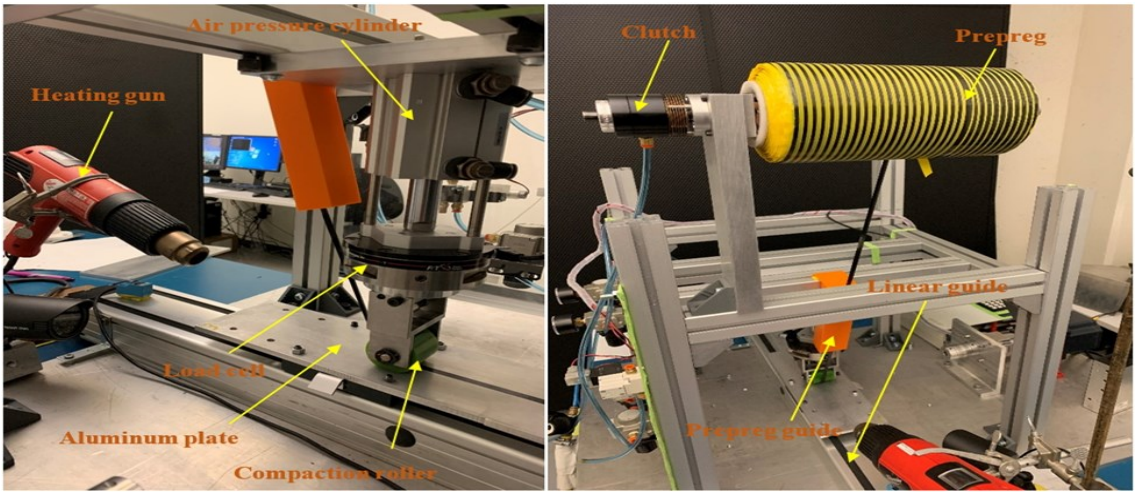

Figure 4.1. Automated layup setup

4.3 Peel Test Setup

The functional principle of this test method has been adapted from the adhesive strength peel test. The peel test setup is illustrated in Figure 4.2. In this setup, a ball-bearing carriage and guide rail are used to hold the aluminum plate. The guide rail is fixed on the lower grip of the tensile machine, while the carriage is connected to the upper grip so they can both move simultaneously. A low-capacity load cell (10 N) is used to record the peel force throughout the test.

The procedure for this peel test is as follows. The prepreg sample is laid-up on the aluminum plate. This plate is immediately transferred to the test machine and fixed on the moving carriage. The free end of the sample is inserted into the machine's upper grip. The crosshead is driven in the tensile direction at 100 mm/sec, and the prepreg sample is peeled from the aluminum plate. Since higher peel force can be obtained by increasing the peel rate [93], this peel rate must remain constant during all experiments according to the peel test standard D6862−11 [94]. The force required to peel the sample is monitored by the load cell. The prepreg tack is considered as the average load per unit width required to peel the prepreg from the substrate. The first 25 mm of the sample is not measured according to the above-mentioned standard; further, every test is performed on three samples laid-up at the same conditions. To study the influence of the process parameters on the prepreg tack, the test is performed on different sets of samples. These sets are laid up by the layup setup at a chosen variation of the process parameters, which include temperature, speed, and compaction force.

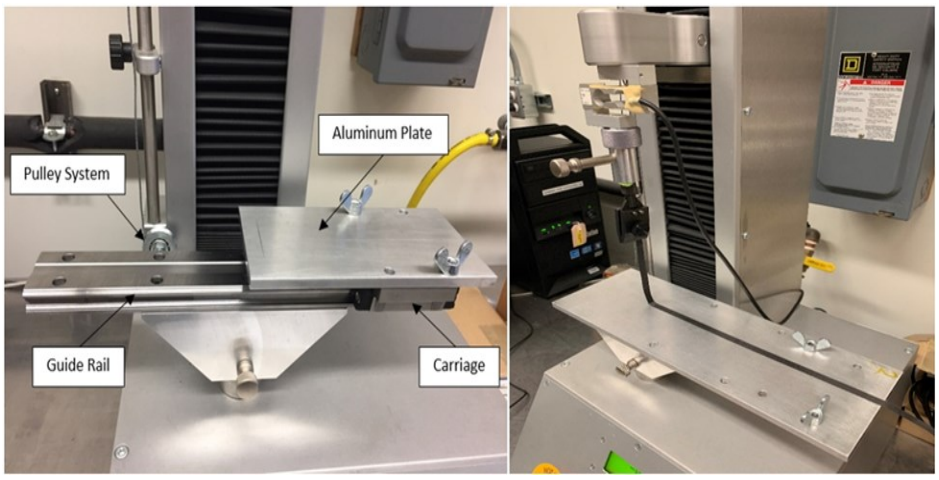

Figure 4.2. Peel test setup

4.4 Design of Experiments (DOE) Using Taguchi Method

Generally, in common factorial methods, a full range series of experiments is performed to understand the effect of every single variable. In this study, three factors need to be investigated, and each factor has four levels. Thus, 64 test combinations must be done, and each test needs to be repeated at least three times to ensure accuracy and experiment repeatability, which leads to a total of 192 tests. Since prepreg properties change by time. Performing this number of tests is not an easy task and has to be minimized. The Taguchi method is an efficient tool for designing a process that operates effectively over a variety of conditions. By using this method, the number of experiments is reduced, while the remaining test data are obtained by the Taguchi prediction. In this method, a three-step approach should be carried out, i.e., selecting the level of each parameter, finding the fitting orthogonal array, and conducting the experiments according to the designed process. Analysis and prediction of data are executed using Minitab and ANOVA DOE [90-92]. This study investigates the influence of three layup process parameters, i.e., heat gun temperature (resin temperature), compaction force, and feed rate on prepreg tack. For each parameter, four levels are selected based on the previous experimental work done by our team. The selected values for each parameter are presented in Table 4.1, while a 60 durometer hard roller (Figure 4.3.a) is used throughout all tests. Since the heat gun is placed 100 mm away from NIP point with a 15^{o} angle, the prepreg temperature will not exceed 60°C. In this case, based on the experiment's design, considering three factors with four levels, the L16 orthogonal array is selected. The experimental process is reported in Table 4.2. Instead of 64 tests, only 16 need to be performed to investigate the effect of each factor by using Minitab. In addition, the Taguchi method can rank factors according to their effectiveness. In this study, heat gun temperature is the most effective factor, while the feed rate is the least.

Table 4.1. Selected layup parameters and their levels

Layup parameter	Unit	Level 1	Level 2	Level 3	Level 4
Heat gun temperature	°C	200	300	400	500
Compaction force	N (lb)	89 (20)	133 (30)	178 (40)	267 (60)
Feed rate	mm/sec	25	50	75	125

Table 4.2. L16 orthogonal array used for experimental design

Sample	Compaction Force (N)	Heat Gun Temperature (°C)	Feed Rate (mm/sec)
1	89	200	25
2	89	300	50
3	89	400	75
4	89	500	125
5	133	200	50
6	133	300	25
7	133	400	125
8	133	500	75
9	178	200	75
10	178	300	125
11	178	400	25
12	178	500	50
13	267	200	125
14	267	300	75
15	267	400	50
16	267	500	25

The optimal conditions of the three parameters are found using the Taguchi prediction. These conditions are not necessarily among the 16 tests mentioned in Table 4.2. After running the entire series, the Taguchi prediction is obtained and compared with the real test results. The first series of experiments investigated the effect of heat gun temperature, feed rate, and compaction force. To investigate the effect of roller type and dwell time, another series of experiments was performed using three different rollers. These rollers, i.e., two polyurethane 60 durometer rollers (hard and perforated) and a stainless-steel roller with low-friction tape, as shown in Figure 4.3, were selected based on their hardness. In the second series of experiments, three levels were selected for each process parameter based on the optimal combination from the first series (Table 4.3). An L9 orthogonal array was selected for this experimental design, where only nine tests were carried out (Table 4.4), while the remaining tests results were generated by Minitab.

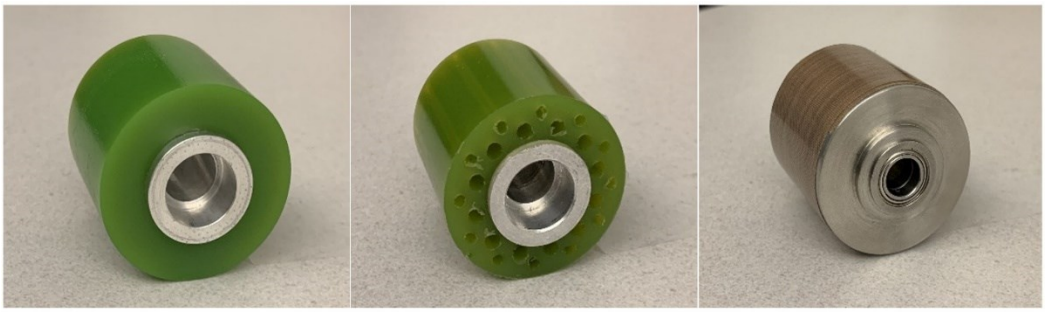

Figure 4.3. (a) 60 durometer; (b) 60 durometer (perforated); (c) stainless-steel roller

Table 4.3. Selected layup parameters and their levels

Layup Parameter	Unit	Level 1	Level 2	Level 3
Roller type		Hard	Perforated	Stainless Steel
Heat gun temperature	°C	350	400	450
Compaction force	N (lb)	89 (20)	133 (30)	178 (40)
Feed rate	mm/sec	25	50	75

Table 4.4. L9 orthogonal array used for experimental design

Sample	Roller	Compaction Force (N)	Heat Gun Temperature (°C)	Feed Rate (mm/sec)
1	Metal	89	350	25
2	Perforated	89	400	50
3	Hard	89	450	75
4	Hard	133	350	50
5	Metal	133	400	75
6	Perforated	133	450	25
7	Perforated	178	350	75
8	Hard	178	400	25
9	Metal	178	450	50

4.5 Taguchi Prediction

The Taguchi method was applied with an L16 orthogonal array for experimental design. The experimental results of the 16 tests (Table 4.2) were analyzed by Minitab and used to predict the remaining 48 test results. Figure 4.4 illustrates part of the obtained results, which are presented in Appendix B. These results show that the highest peel force, which corresponds to the highest tack level, is obtained at 400°C heat gun temperature, 178 N (40 lb) compaction force, and 50 mm/sec feed rate. On the other hand, the lowest tack level was found at 200°C heat gun temperature, 89 N (20 lb) compaction force, and 125 mm/sec feed rate. The results also revealed that heat gun temperature has the greatest effect on prepreg tack among the three selected parameters, as depicted in Figure 4.5. The results for each parameter will be discussed separately in the next sections.

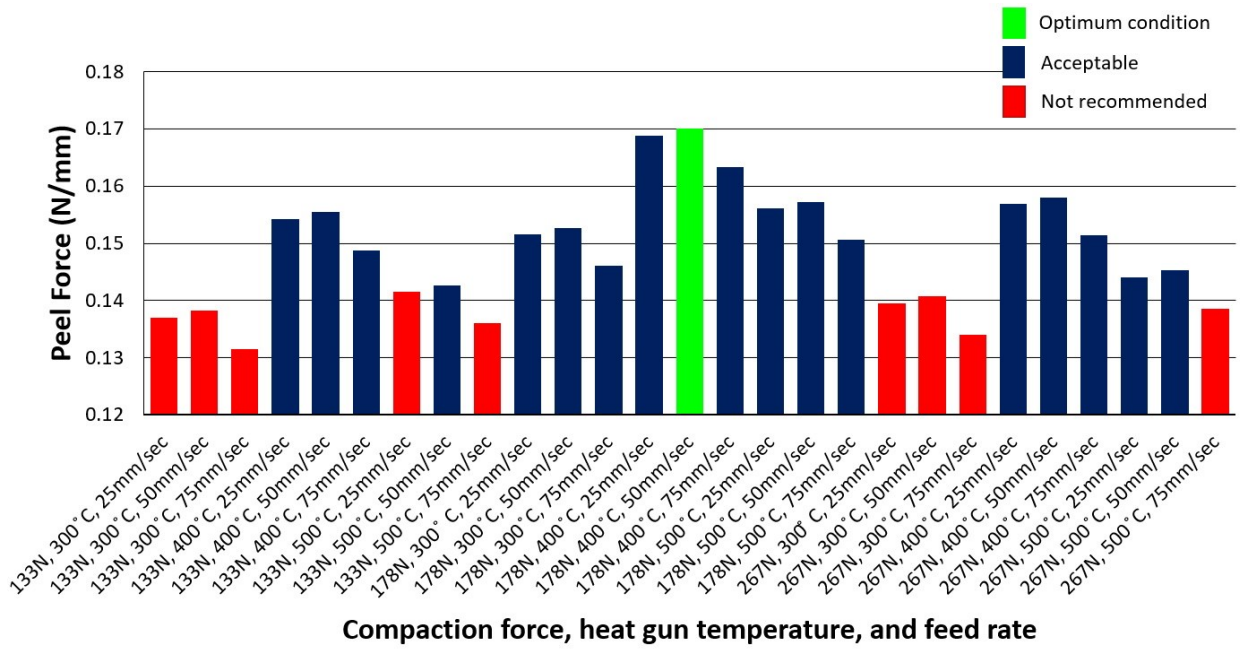

Figure 4.4. Peel force predicted by Taguchi method with the corresponding process parameters

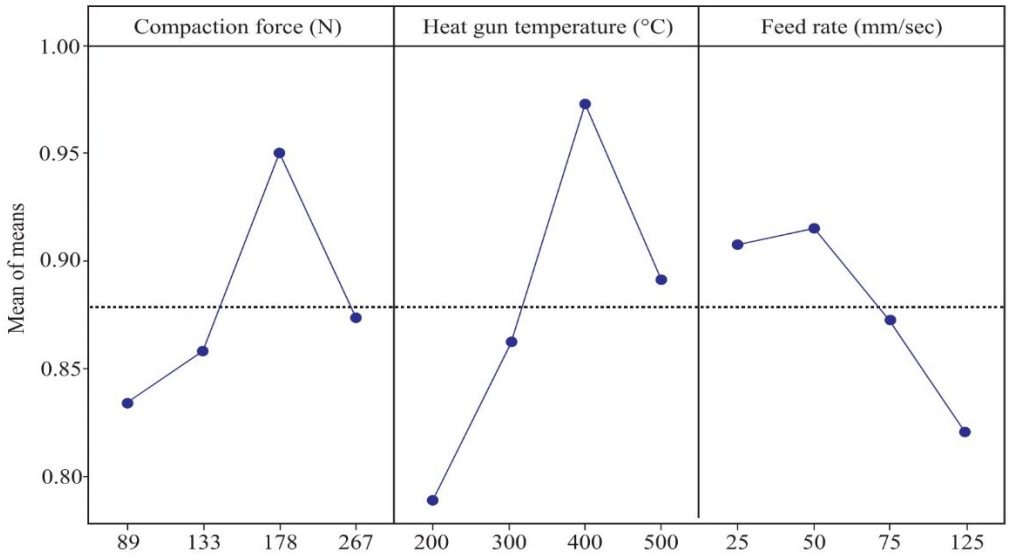

Figure 4.5. Effect of each process parameter on peel force based on Taguchi method results

4.6 Confirmation Tests

The optimal level of the layup parameters selected by Minitab software was not among the 16 tests that were performed. Thus, to prove the selected combination of parameters experimentally, a layup process was accomplished at 400°C heat gun temperature, 178 N (40 lb) compaction force, and 50 mm/sec feed rate followed by peel test. Figure 4.6 depicts the optimal peel force achieved by applying these process parameters compared to the predicted one. The results revealed good agreement between the two values around 5.4%, which demonstrates that the Taguchi method is an appropriate tool for such process parameter optimization.

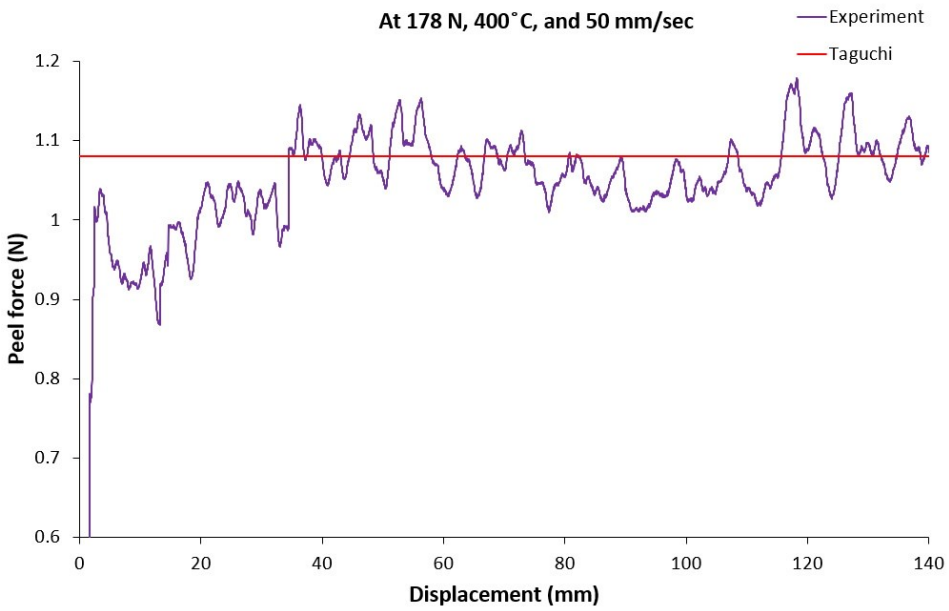

Figure 4.6. Peel force at the optimum conditions (experiment and Taguchi prediction)

4.7 Effect of Process Parameters

4.7.1 Heat Gun Temperature

Results show that the effect of temperature on peel force is greater than the effect of the other two parameters (Figure 4.5). This demonstrates the temperature as a key factor in the layup process to obtain a sufficient tack level. The effect of temperature on tackiness is correlated to its impact on the viscoelastic behavior of the resin. Increasing the prepreg temperature leads to decreasing resin viscosity; consequently, better intimate contact is achieved. However, results show that increasing temperature improves prepreg tackiness up to a certain peak point; exceeding this temperature deteriorates prepreg tackiness. This tackiness decline is due to the extreme decrease of resin viscosity, which is accompanied by a drop in resin strength. In the peel test, two different failure modes were observed during the debonding process (Figure 4.7.a). The first type is the dry interfacial failure. This failure occurs at temperatures lower than the peak and refers to adhesive

failure. The second failure mode is the cohesive failure, which happens when resin loses its strength at temperatures higher than the peak. This failure mode can be noticed by the remaining print of resin on the tool surface, as illustrated in Figure 4.7.b. To have a strong bond, the resin should be viscous enough to move and stick to the substrate. In parallel, it should be strong enough to resist separation before peeling from the substrate. Figure 4.8 presents the average measured peel force at different sets of process parameters; further each set has four different temperatures, which indicates that peel force at 400°C is the highest throughout all the sets.

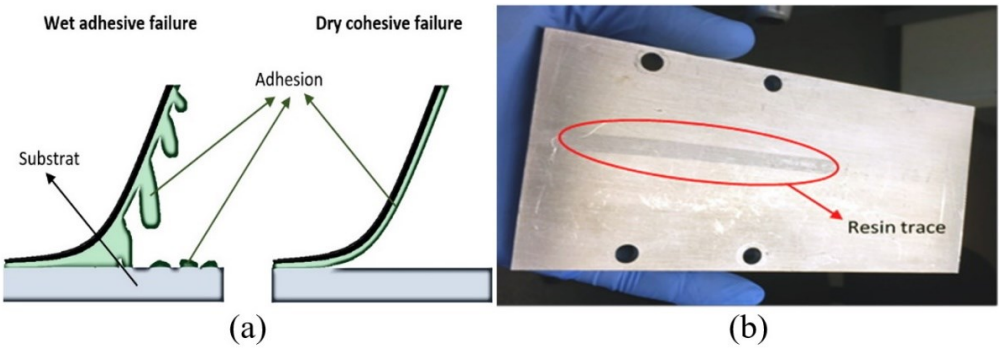

Figure 4.7. (a) Failure types at adhesive peel test. (b) Resin trace caused by a wet adhesive failure

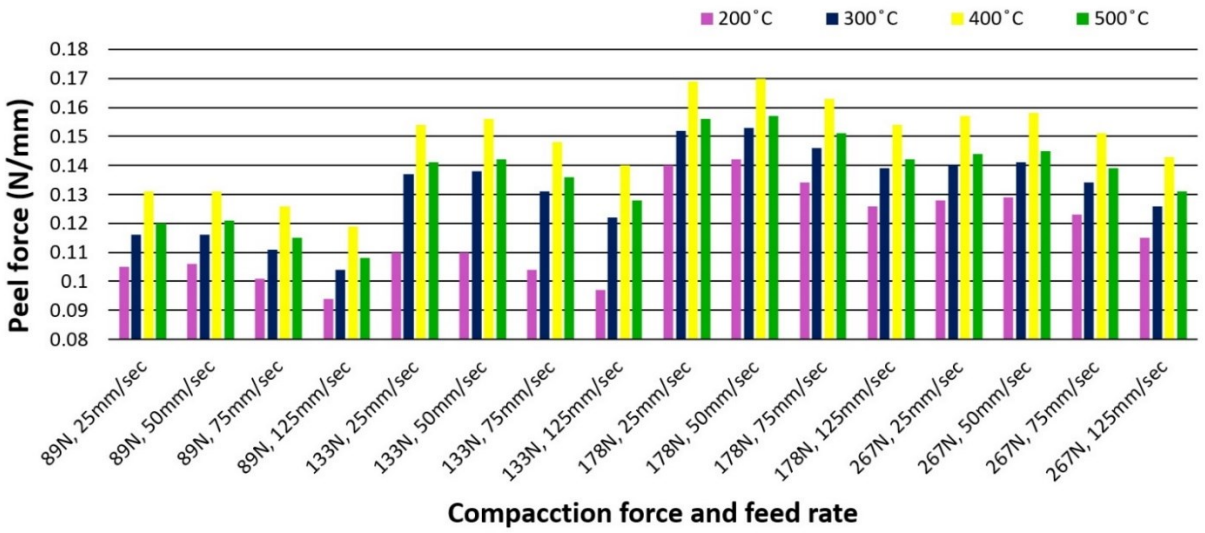

Figure 4.8. Peel force per unit width for different heat gun temperatures and the corresponding process parameters

4.7.2 Feed Rate

Results show that the feed rate influence on peel force is the lowest compared with the effect of temperature and compaction force (Figure 4.5). However, its effect is considerably high. Figure 4.10 shows that increasing the feed rate from 25 to 125 mm/sec decreases the peel force by 20%. It was observed that low and high feed rates have a similar effect of high and low temperatures on peel force, respectively. At low feed rate, the resin has enough time to be heated, move to the interface area, and provide good tackiness. Inversely, a high feed rate reduces that time and has a negative impact on the tack level. Besides, this high-speed effect is attributed to the resulted short dwell time. However, moving slower than a certain speed causes too much pressure and heat on the resin, which degrades the resin properties and reduces the prepreg tack. Selecting the appropriate feed rate is directly related to the other parameters. In the case of low feed rate, high temperature and compaction force need to be avoided.

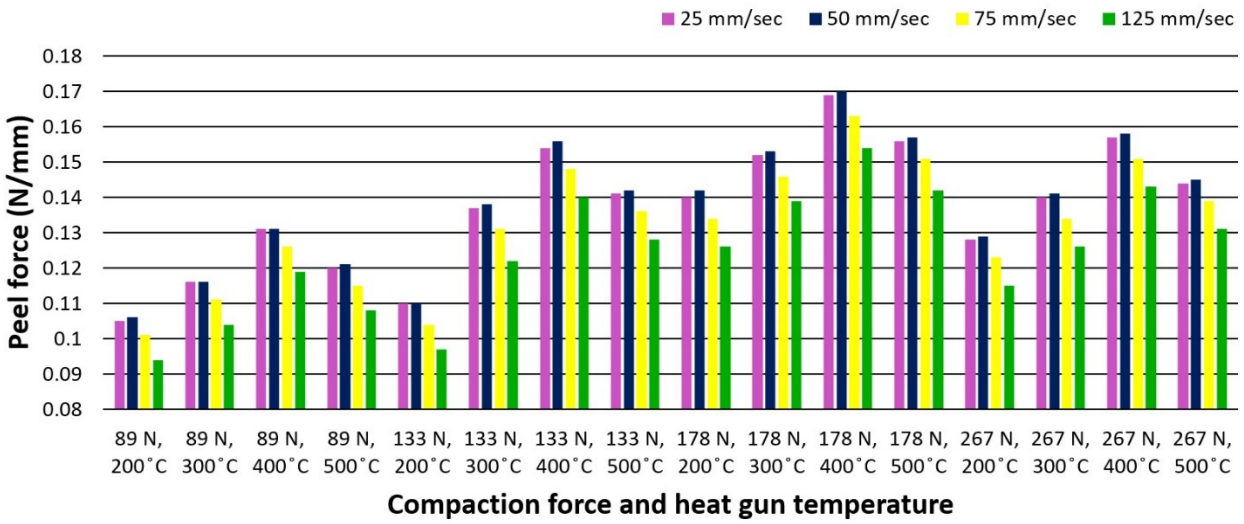

Figure 4.9. Peel force per unit width for different feed rates and the corresponding process parameters

Results show that the maximum tack is obtained at high temperatures and high feed rates. Reducing temperature shifts the process toward a low feed rate, as more time is required for the prepreg to be properly heated and bonded to the substrate. On the other hand, low feed rate gives better results with low compaction force than with a high one. Figure 4.10 indicates a fluctuation in the graph at the higher speed, which is attributed to the force inconsistency caused by increasing the layup speed. This force variation helps the formation of local buckling in areas with low tack levels, which leads to premature failure. Figure 4.9 shows that 50 mm/sec speed gives the best results among all tests with a slight difference from 25 mm/sec.

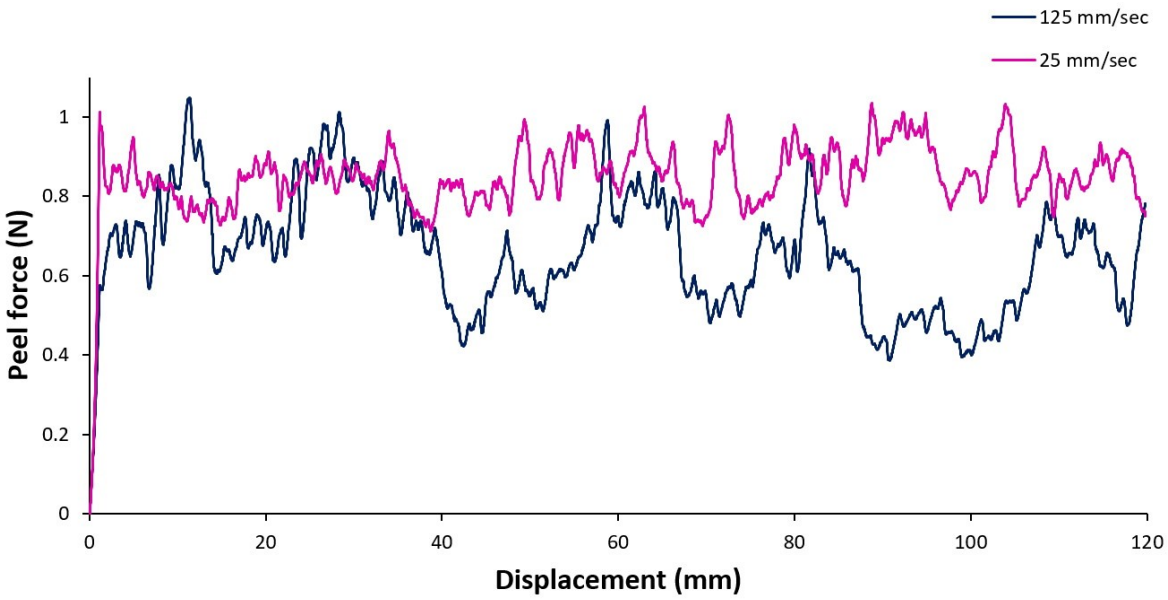

Figure 4.10. Peel force fluctuation at two different feed rates

4.7.3 Compaction Force

Results show that peel force is significantly improved by increasing the compaction force. The purpose of the pressure applied by a compaction roller is to facilitate bonding between prepreg and substrate. This pressure enforces more resin migration through the prepreg to the interface area; thus, a high tack level is achieved. Figure 4.12 indicates that 178 N (40 lb) force generates the maximum peel force with a clear difference compared with the other forces. It also shows that exceeding this force has a negative impact on peel force. The high pressure applied on prepreg tends to reduce the resin content at the interface area and, hence, decreases the prepreg tack. Moreover, it affects the prepreg geometry and fiber distribution as well. Figure 4.13 depicts a laid-up prepreg with a high compaction force 445 N (100 lb), where the prepreg width increased by almost 3 mm. For that reason, the prepreg width has to be monitored throughout the tests, and the peel force is reported per unit width. The roller used in this study is made of polyurethane (35 durometer). Figure 4.11.b indicates the contact area under two different compaction forces; further,

the roller deformation is plotted against the applied force in Figure 4.11.a. Increasing contact area develops better load distribution and enhances tackiness if enough load is applied.

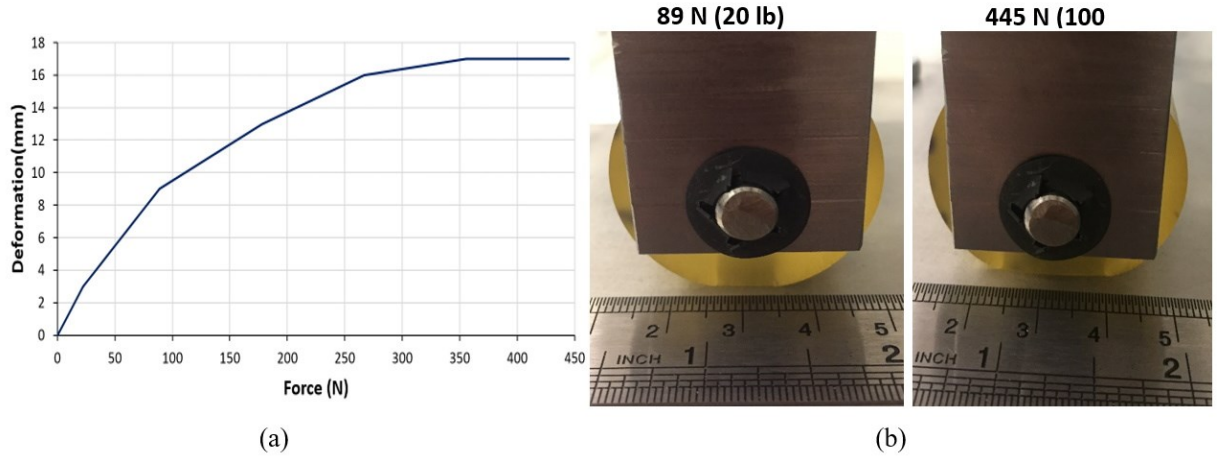

Figure 4.11. (a) Roller deformation vs. static pressure. (b) Roller deformation at two different loads

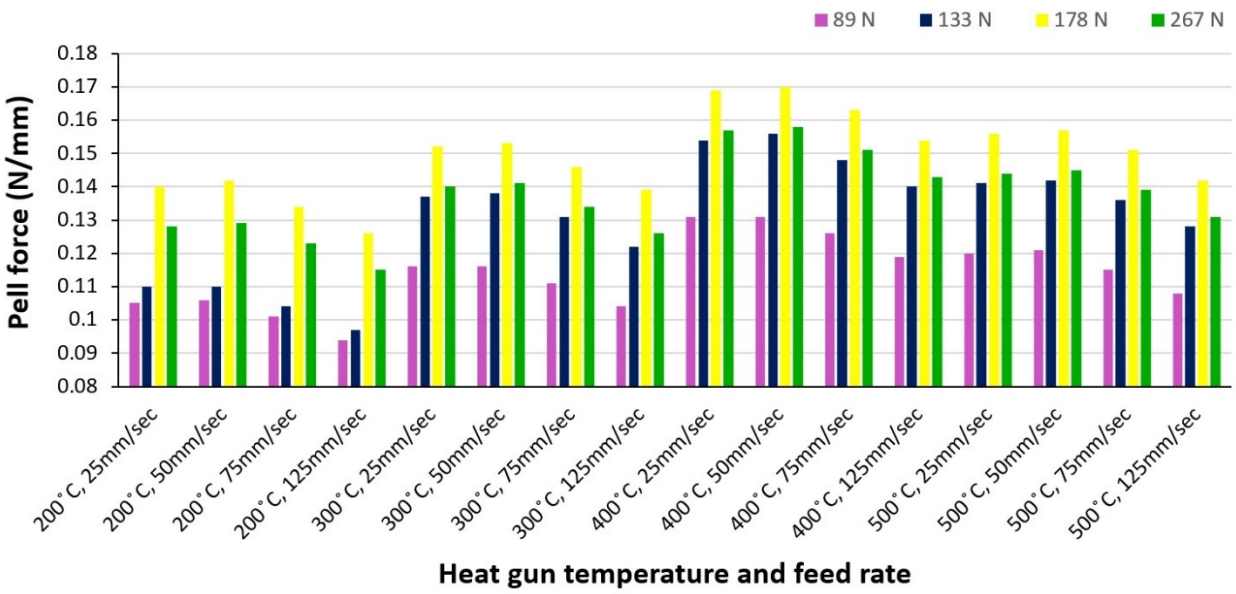

Figure 4.12. Peel force per unit width for different compaction forces and the corresponding process parameters

Figure 4.13. Prepreg expansion under a high compaction force (445 N)

4.8 Effect of Placing Roller

4.8.1 Taguchi Prediction and Confirmation Tests

To study the influence of the placing roller on peel force, the Taguchi method was used for the design of experiment and to predict the results for each roller using an L9 orthogonal array. Three different rollers were used in this study, i.e., two polyurethane 60 durometer rollers (hard and perforated) and a stainless-steel roller with low-friction tape (Figure 4.3). Nine sets of tests were performed (Table 4.4), while the results of the remaining tests were analyzed and obtained using Minitab software. Figure 4.14 presents the results of all 27 sets of tests, indicating the resultant peel force for each set. The results reveal that the hard roller was slightly better than the other two rollers; further, the maximum peel force was achieved by this roller at 400°C heat gun temperature, 178 N (40 lb) compaction force, and 25 mm/sec feed rate; whereas the lowest peel force was reported for the metal roller at 350°C heat gun temperature, 178 N (40 lb) compaction force, and 75 mm/sec feed rate. The difference between the two rollers is mainly attributed to the line contact area of the metal roller. Moreover, due to the appropriate dwell time, the highest peel force for all the rollers was observed at the lowest feed rate (25 mm/sec). The metal roller demonstrated a low peel force at the highest compaction force due to its impact on the resin content and geometry.

However, at low compaction forces, the metal roller showed as high peel force as the hard roller. Table 4.5 presents the highest and lowest peel force for each roller with the corresponding process parameters.

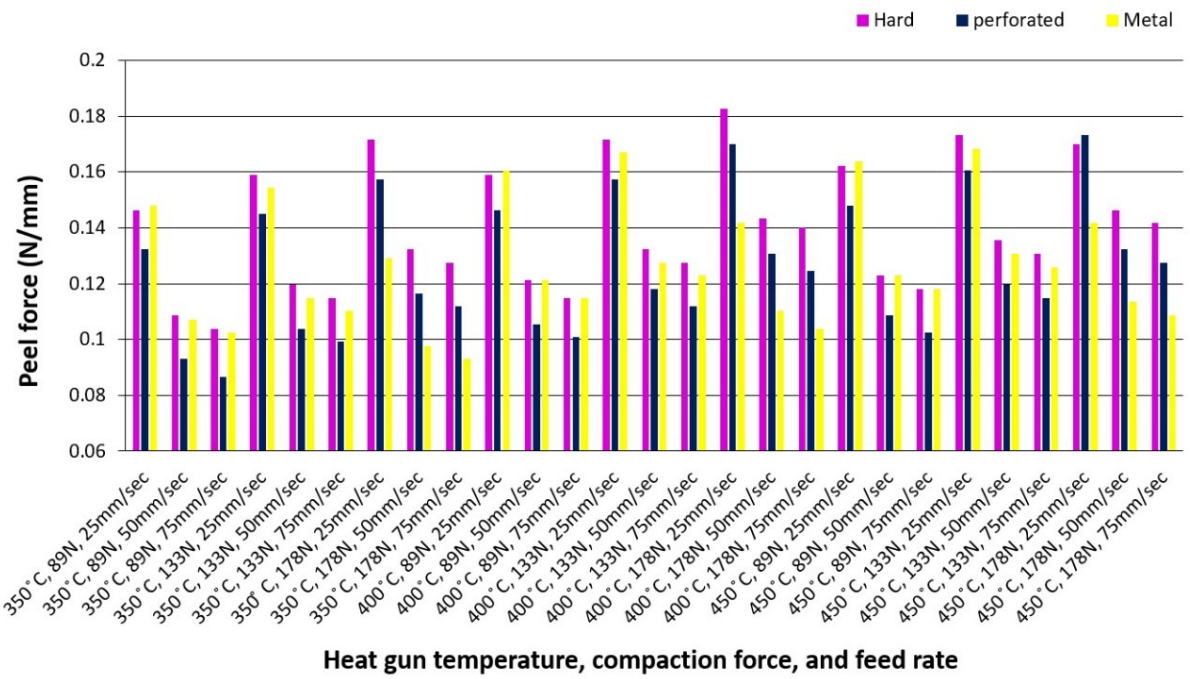

Figure 4.14. Predicted peel force results for three different rollers and the corresponding process parameters

Table 4.5. Highest and lowest peel force for each roller and corresponding process parameters.

Roller	Heat gun temperature (°C)	Compaction force (N)	Feed rate (mm/sec)	Highest peel force (N/mm) Lowest Peel Force (N/mm)
Metal	450	133	25	0.164
	350	178	75	0.092
Hard	400	178	25	0.182
	350	89	75	0.104
perforated	450	178	25	0.173
	350	89	75	0.086

To verify the predicted results, three sets of experiments were selected (see Table 4.4) for each roller. The results of the performed tests were compared with the predicted results from the Taguchi method (Figure 4.15). Good agreement between the experimental and predicted results was revealed for all roller types. Good agreement with a percent difference of 1.5-5% between the experimental and predicted results was revealed for the three rollers. The figure indicates a different fluctuation with each roller as more fluctuation with the metal roller and less with the perforated one. This difference is attributed to the hardiness and the load distribution of each roller.

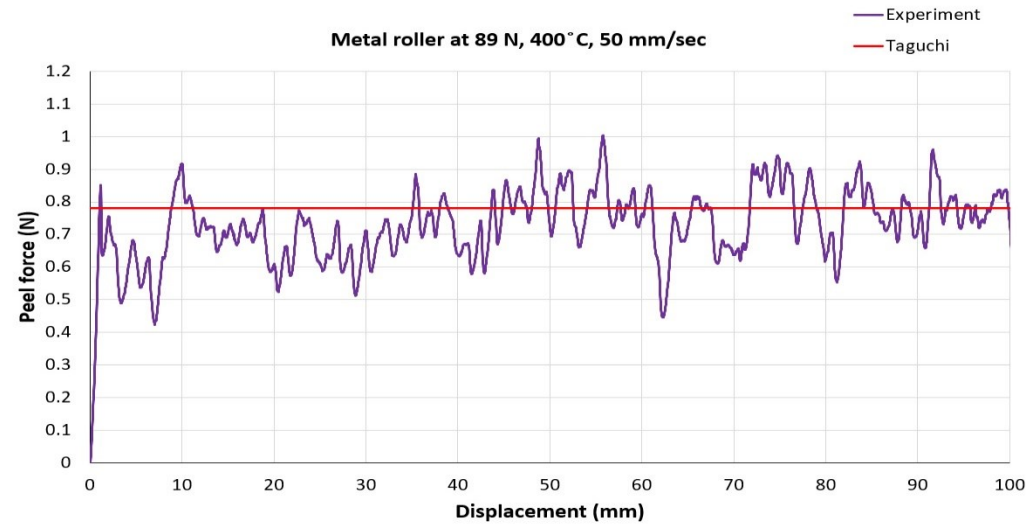

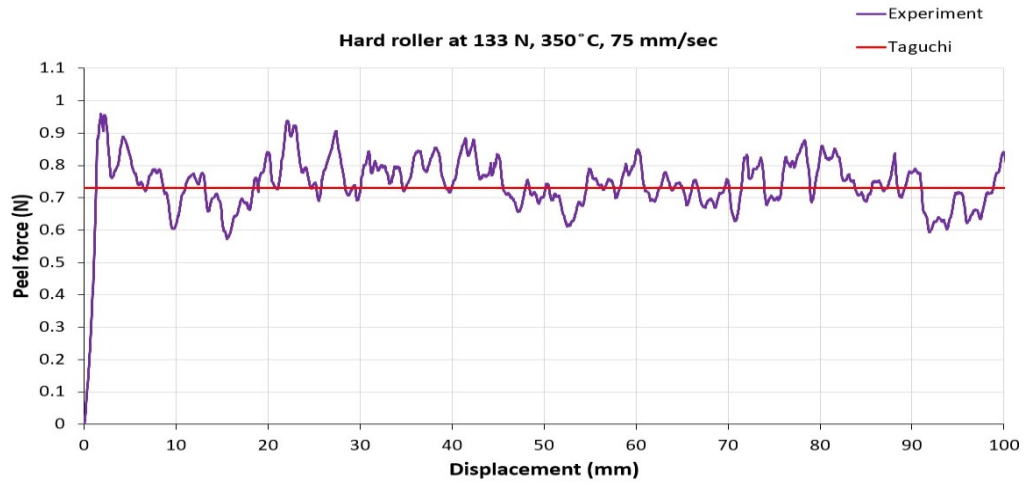

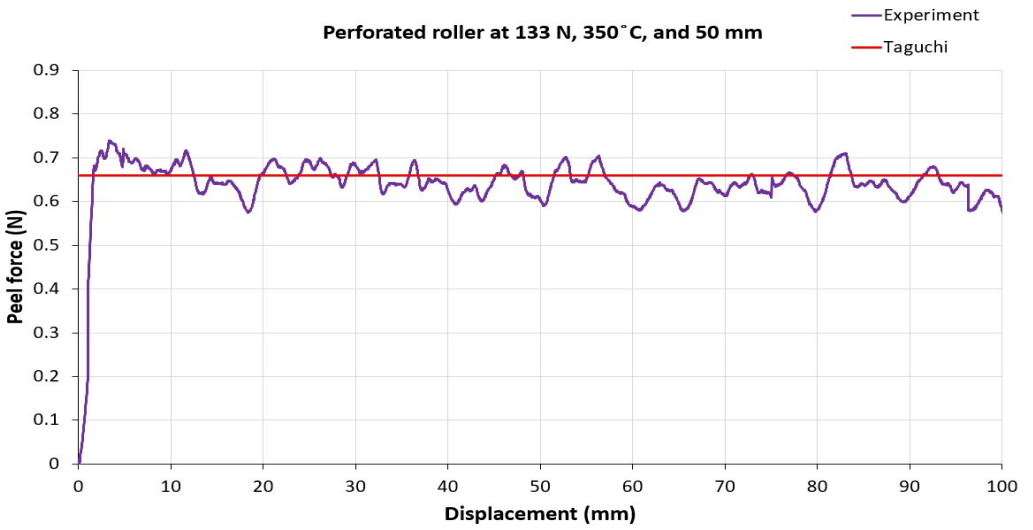

Figure 4.15. Peel force for three different rollers at three different sets of process parameters (experiment and Taguchi prediction)

4.8.2 Roller Effect at Different Compaction Forces

The applied force in the layup process causes roller deformation, which consequently affects dwell time and compaction pressure. To discuss the roller effect on peel force, the results are presented at three different compaction forces (Figures 4.16-18). These results show that, at 89 N (20 lb) compaction force and 25 mm/sec feed rate, the metal roller demonstrated the highest peel force with a slight difference from the hard one. The metal roller does not undergo any deformation, and the contact area is nothing but close to a line. As a result, the metal roller generates the highest pressure on the prepreg among the three rollers. The hard and perforated rollers have a larger deformation and wider contact area than the metal one; consequently, the pressure applied by the two rollers is lower, and the peel force is less. The perforated roller showed the lowest peel force results, as depicted in Figure 4.16; in addition, these low peel force values are attributed to its larger deformation, which leads to a lower pressure distribution. At higher feed rates (50 and 75 mm/sec), there was an obvious drop in the peel force for the three rollers, which is attributed to the short time the rollers remain in contact with the prepreg.

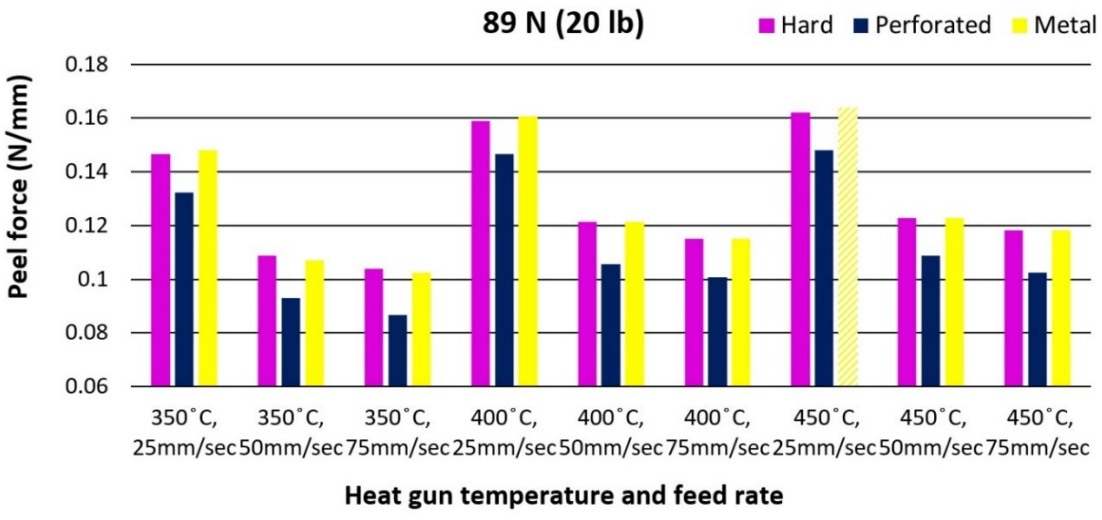

Figure 4.16. Peel force per unit width at 89 N compaction forces and the corresponding process parameters (optimum condition highlighted)

The results reveal an overall improvement in peel force of samples laid-up at 133 N (30 lb) compaction force (Figure 4.17). Once again, the lowest peel force values were reported at higher feed rates (50 and 75 mm/sec), while the highest peel force values were indicated at 25 mm/sec feed rate. The hard roller showed the best results among the three rollers due to the sufficient pressure distribution and dwell time compared with the low pressure of the perforated one and the pressure applied by the metal one.

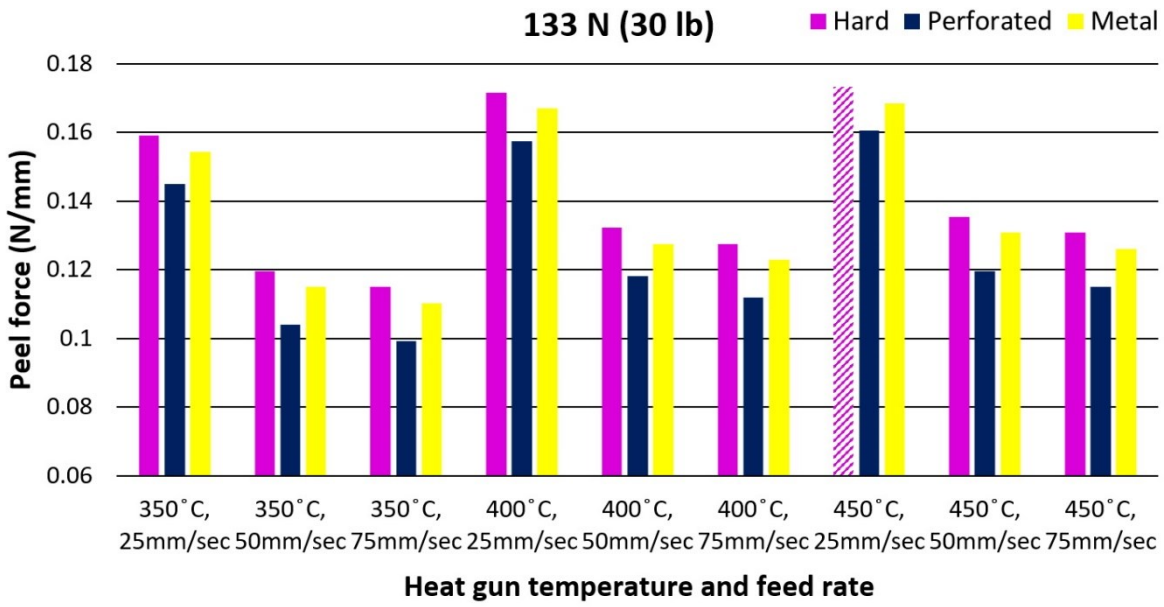

Figure 4.17. Peel force per unit width at 133 N compaction forces and the corresponding process parameters (optimum condition highlighted)

At 178 N (40 lb) compaction force, the metal roller experienced a significant decrease in the corresponding peel force values (Figure 4.18). This is due to the high amount of resin forced to move through the prepreg cross-section to the plate by the high compaction load. Therefore, for the metal roller, increasing compaction force more than 133 N (30 lb) diminishes the resin's properties and reduces the prepreg tackiness. The highest peel force recorded at this compaction force was at 400°C and 25 mm/sec for a sample laid-up by the hard roller due to the higher

distributed load on the sample. The results demonstrate a consistent advantage of the hard roller over the perforated one throughout all the tests except one case. At 450°C and 25 mm/sec, the perforated roller showed a higher peel force than the other rollers, which indicates that the influence of the perforated roller long dwell time overcomes the high load of hard roller.

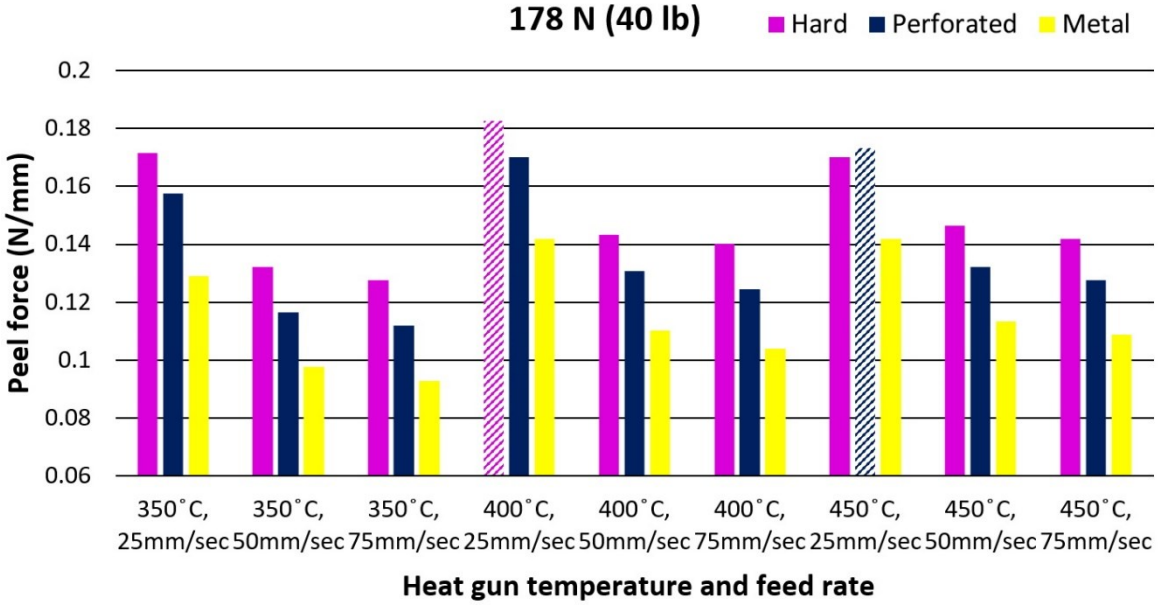

Figure 4.18. Peel force per unit width at 178 N compaction forces and the corresponding process parameters (optimum condition highlighted)

4.9 Summary

In this study, the AFP process was performed using an in-house setup, which can readily change the process parameters. The prepreg tack was identified by the peel force required to separate the prepreg from the substrate, as measured by a 90° peel test. The experiments were limited only to the first layer, where a high tack level is required to ensure a good bond between prepreg and the tool. The effect of the main process parameters, i.e., compaction force, heat gun temperature, and feed rate on peel force (prepreg tack), was comprehensively investigated. In addition, the influence of the placing roller was also examined by using three different rollers. The Taguchi method was

employed to determine the optimal values of the process parameters. These optimal values were experimentally confirmed. The optimal combination of the process parameters predicted by the Taguchi method was 400°C heat gun temperature, 178 N (40 lb) compaction force, and 50 mm/sec feed rate using the hard 60 durometer roller. It was found that increasing heat gun temperature to a certain level reduces prepreg tack. For the feed rate, the optimal results were obtained at 50 mm/sec, while lower and higher feed rate values provided a lower tack due to the excessive load and short dwell time, respectively. Results revealed better tackiness with higher compaction force with a certain limit, as it helps resin movement and facilitates bonding. For the roller effect on tackiness, it has been determined that a hard roller reported better results compared with the other two rollers. However, it was observed that changing the compaction force has a major impact on the roller effect.

Chapter 5: Conclusion and Future Work

5.1 Conclusion

This work is motivated by the significant improvement that steering applies to the mechanical properties of composite structures. In this thesis, out-of-plane wrinkling as one of the most effective defects during steering thermosetting prepreg using automated fiber placement is investigated. First, a theoretical model of an isolated wrinkle is developed using Rayleigh–Ritz approach based on the critical buckling load. Unlike the previous models, Pasternak elastic foundation is implemented to represent the interaction between the steered prepreg and the substrate with a shear layer. This model provides a closed-form solution to accurately predict the critical steering radius, which can be laid-up with no wrinkles. It also can predict the wrinkles wavelength if the steering radius is lower than the critical one.

In addition, the validation of the theoretical model is carried out by various experimental AFP trials. The prepreg is steered with different steering radii at the same process parameters. All the steered tapes are examined for wrinkles existence, and wrinkles are counted for measuring the wrinkles wavelength. Moreover, the Pasternak foundation's two parameters are experimentally characterized using two different methods. The normal stiffness is characterized by performing a probe tack test, while bias extension method is used to characterize the shear stiffness. Finally, the experimental observations are compared to the output of the mechanical model. The comparison shows a good agreement and prediction improvement over the other available models. This model reveals a high prediction accuracy, which can help composite engineers to take full advantage of steering, improve steering quality, and enhance the design flexibility.

A new prepreg peel test setup is designed to study the prepreg tack as one of the most effective factors on the steering defects formation. The average peel force is used as an indicator of the tack level. Another setup is designed to imitate the AFP process with full control of the process parameters, and lay-up the samples tested by the peel test setup. These two setups are employed to study the impact of the main three process parameters: processing temperature, lay-up speed and compaction force. They are also used to study the influence of placing rollers using three different rollers. Taguchi method is employed for design of experiments (DOE) to determine the optimal values of the process parameters. L16 orthogonal array is used for the abovementioned three process parameters, while L9 orthogonal array is used for the influence of the placing roller. The optimal values determined by Taguchi method are experimentally confirmed. Processing temperature indicated the highest impact on tack level among the three parameters. However, the overall results proved that interaction between different process parameters has also a high impact on tack level as the individual impact of each parameter.

5.2 Future Work

Considering this work and the related studies in the literature, the following recommendations can be stated for future work within this field of research.

- Aside from out-of-plane wrinkling, in-plane waviness has been also observed throughout the experimental work. This defect should be more highlighted in the coming steering related studies.
- Shear properties of non-cured thermoset prepreg should be characterized using appropriate methods that provide a sufficient deformation rates representing the real manufacturing process.

- Steering defects including out-of-plane wrinkles have to be investigated post lay-up process. For example, the development of the defected areas during curing process and the impact of these defects on the properties of the final structure.
- Prepreg tack has shown high sensitivity to all studied process parameters. To have a better understanding of this property, more process parameters as well as environmental factors such as tool surface roughness and humidity should be included in the related studies.

5.3 Contributions

The original contributions of this thesis concern the formation of out-of-plane wrinkles as one of the manufacturing defects that occur on the steered thermosetting prepreg. In summary, the main contributions are:

- An analytical model to investigate the wrinkle formation during steering in AFP is developed. This model can predict the critical steering radius and the wrinkles wavelength.
  - Experimental work is performed by AFP to validate this model.
- A simple experimental approach is introduced to characterize the foundation parameters including normal and shear stiffness.
- A new peel test to measure the prepreg tack is designed based on the average peel force.
- The effect of process parameters on the prepreg tack is investigated, these parameters include temperature, lay-up speed and compaction force.
- An optimal process parameters combination is obtained by applying the Taguchi method to the experimental results.

In addition to the above reported contributions, the following publications have been accomplished during the study:

Journals:

- **M. Belhaj** and M. Hojjati. Wrinkle formation during steering in automated fiber placement: Modeling and experimental verification. *Journal of Reinforced Plastics and Composites*, 37:396–409, 2018.
- **M. Belhaj**, A. Dodangeh and M. Hojjati. Experimental Investigation of Prepreg Tackiness in Automated Fiber Placement. *Composite Structures,* 262:113602,2021.

Conferences:

- **M Belhaj**, N Bakhshi and M Hojjati. Foundation parameters characterization for prediction of critical steering radius in Automated Fiber Placement. *17th European conference on Composite Materials, ECCM,* Athens, Greece, 2018.
- N Bakhshi, **M Belhaj** and M Hojjati. Viscoelastic effects on wrinkle formation during tow steering in Automated Fiber Placement. *17th European conference on Composite Materials, ECCM,* Athens, Greece, 2018.
- **M Belhaj**, H Alshahrani and M Hojjati. Influence of foundation parameters on steering radius during AFP. *15th Japan International SAMPE Symposium & Exhibition (JISSE15)*, Tokyo, Japan, 2017.

Bibliography

[1] D. D. L. Chung, *Composite materials: science and applications*. Springer Science & Business Media, 2010.

[2] Boeing, "787 Aircraft Rescue & Firefighting Composite Structure," accessed 21-September-2019.

[3] S. V. Hoa, *Principles of the manufacturing of composite materials.* DEStech Publications, Inc, 2009.

[4] Slideshare website.< www.slideshare.net/gauravkumarkarnawat/manufacture-of-composites-59038466>.

[5] Automated Dynamics website.<www.automateddynamics.com/article/thermoplastic-composite-basics/processing-methods/automated-fiber-placement>.

[6] A. Lewis, "Making composite repairs to the 787," *Aero Online*, vol. Qtr 4, no. 56, pp. 5–13, 2014.

[7] C. González, J. J. Vilatela, J. M. Molina-Aldareguía, C. S. Lopes, and J. LLorca, "Structural composites for multifunctional applications: Current challenges and future trends," *Progress in Materials Science*, vol. 89, pp. 194–251, 2017.

[8] D. H. J. a Lukaszewicz, C. Ward, and K. D. Potter, "The engineering aspects of automated prepreg layup: History, present and future," *Composites Part B: Engineering*, vol. 43, no. 3, pp. 997–1009, 2012.

[9] J. Sloan, "ATL and AFP: Signs of evolution in machine process control," *High-Performance Composites*, vol. 2, pp. 417–47, 2008.

[10] T. Gutowski, *Advanced composites manufacturing*. Wiley, 1997.

[11] F. C. Campbell, *Manufacturing processes for advanced composites*. Elsevier, 2003.

[12] B. T. Åström, *Manufacturing of polymer composites*. CRC press, 2018.

[13] D. O. Evans, Fiber placement. In *Handbook of Composites*, pp. 476-487. Springer, 1998.

[14] Y. Di Boon, S. C. Joshi, and S. K. Bhudolia, "Recent advances on the design automation for performance-optimized fiber reinforced polymer composite components," *Journal of Composites Science*, vol. 4, no. 2, pp. 61, 2020.

[15] J. Frketic, T. Dickens, and S. Ramakrishnan, "Automated manufacturing and processing of fiber-reinforced polymer (FRP) composites: An additive review of contemporary and modern techniques for advanced materials manufacturing," *Additive Manufacturing*, vol. 14, pp. 69–86, 2017.

[16] B. Denkena, C. Schmidt, and P. Weber, "Automated fiber placement head for manufacturing of innovative aerospace stiffening structures," *Procedia Manufacturing*, vol. 6, pp. 96–104, 2016.

[17] Anon, *MIL-HDBK-17-3F: Composite materials handbook*. Technomic, 2002.

[18] G. Marsh, "Automating aerospace composites production with fibre placement," *Reinforced plastics*, vol. 55, no. 3, pp. 32–37, 2011.

[19] K. Kozaczuk, "Automated fiber placement systems overview," *Prace Instytutu Lotnictwa*, vol. 245, pp. 52–59, 2016.

[20] Z. Gurdal and R. Olmedo, "In-plane response of laminates with spatially varying fiber orientations - Variable stiffness concept," *AIAA journal*, vol. 31, no. 4, pp. 751-758,

1993.

[21] C. S. Lopes, Z. Gürdal, and P. P. Camanho, "Variable-stiffness composite panels: Buckling and first-ply failure improvements over straight-fibre laminates," *Computers & Structures*, vol. 86, pp. 897–907, 2008.

[22] C. Waldhart, *Analysis of tow-placed, variable-stiffness laminates*. Phd thesis, Virginia Tech, 1996.

[23] C. Kassapoglou and G. Zafer, "Design of fiber-steered variable-stiffness laminates based on a given lamination parameters distribution," in *52nd AIAA/ASME/ASCE/AHS/ASC Structures, Structural Dynamics and Materials Conference 19th AIAA/ASME/AHS Adaptive Structures Conference 13t*, p. 1894. 2011.

[24] R Olmedo and Z Gurdal, "Buckling response of laminates with spatially varying fiber orientations," in *34th Structures, Structural Dynamics and Materials Conference*, p. 1567. 1993.

[25] M. Rouhi, H. Ghayoor, S. V. Hoa, and M. Hojjati, "Effect of structural parameters on design of variable-stiffness composite cylinders made by fiber steering," *Composite Structures*, vol. 118, pp. 472–481, 2014.

[26] M. Rouhi, H. Ghayoor, S. V. Hoa, and M. Hojjati, "Multi-objective design optimization of variable stiffness composite cylinders," *Composites Part B: Engineering*, vol. 69, pp. 249–255, 2015.

[27] D. Jegley, B. Tatting, and Z. Gurdal, "Tow-steered panels with holes subjected to compression or shear loading," In *46th AIAA/ASME/ASCE/AHS/ASC Structures,*

Structural Dynamics and Materials Conference, p. 2081. 2005.

[28] C. S. Lopes, Z. Gurdal, and B. F. Tatting, "Progressive failure analysis of tow-placed , variable-stiffness composite panels," *International Journal of Solids and Structures*, vol. 44, pp. 8493–8516, 2007.

[29] C. S. Lopes, *Damage and failure of non-conventional composite laminates*. PhD Thesis, Delft University of Technology, 2009.

[30] C. Fagiano, *Computational modeling of tow-placed composite laminates with fabrication features*. PhD Thesis, Delft University of Technology, 2010.

[31] D. M. J. Peeters, G. G. Lozano, and M. M. Abdalla, "Effect of steering limit constraints on the performance of variable stiffness laminates," *Computers & Structures*, vol. 196, pp. 94–111, 2018.

[32] G. Clancy, D. Peeters, V. Oliveri, D. Jones, R. M. O'Higgins, and P. M. Weaver, "A study of the influence of processing parameters on steering of carbon Fibre/PEEK tapes using laser-assisted tape placement," *Composites Part B: Engineering*, vol. 163, pp. 243–251, 2019.

[33] M. K. Chea, *Investigating in-plane shear behaviour of uncured unidirectional prepreg tapes*, Master's thesis, KTH Royal Institute of Technology, 2019.

[34] K. Potter, B. Khan, M. Wisnom, T. Bell, and J. Stevens, "Variability, fibre waviness and misalignment in the determination of the properties of composite materials and structures," *Composites Part A: Applied Science and Manufacturing*, vol. 39, no. 9, pp. 1343–1354, 2008.

[35] F. Heinecke and C. Willberg, "Manufacturing-induced imperfections in composite parts manufactured via automated fiber placement," *Journal of Composites Science*, vol. 3, no. 2, p. 56, 2019.

[36] B. C. Kim, K. Potter, and P. M. Weaver, "Multi-tow shearing mechanism for high-speed manufacturing of variable angle tow composites," in *15th European Conference on Composite Materials,* 2012.

[37] M. P. Wiehn and R. D. Hale, "Low cost robotic fabrication methods for tow placement," in *47th International SAMPE Symposium and Exhibition*, *2002*.

[38] S. Nagendra, S. Kodiyalam, J. Davis, and V. Parthasarathy "Optimisation of tow fiber paths for composite design," in *36th Structures, Structural Dynamics and Materials Conference*, 1995.

[39] R. P. Smith, Z. Qureshi, R. J. Scaife, and H. M. El-dessouky, "Limitations of processing carbon fibre reinforced plastic / polymer material using automated fibre placement technology," *Journal of Reinforced Plastics and Composites,* vol. 35, no. 21, pp. 1527–1542, 2016.

[40] C. Zhao, J. Xiao, W. Huang, and X. Huang, and S. Gu, "Layup quality evaluation of fiber trajectory based on prepreg tow deformability for automated fiber placement," *Journal of Reinforced Plastics and Composites*, vol. 35, no. 21, pp. 1576–1585, 2016.

[41] H. M. Hsiao and I. M. Daniel, "Effect of fiber waviness on stiffness and strength reduction of unidirectional composites under compressive loading," *Composites science and technology*, vol. 56, no. 5, pp. 581–593, 1996.

[42] A. Caiazzo, M. Orlet, H. McShane, L. Strait, and C. Rachau, “The effects of marcel defects on composite structural properties,” In *Composite structures: theory and practice*. ASTM International, 2001.

[43] T. A. Bogetti, J. W. Gillespie Jr, M.A. Lamontia, “Influence of ply waviness on the stiffness and strength reduction on composite laminates,” *Journal of Thermoplastic Composite Materials*, vol. 5, no. 4, pp. 344–369, 1992.

[44] R. F. El-Hajjar and D. R. Petersen, “Gaussian function characterization of unnotched tension behavior in a carbon/epoxy composite containing localized fiber waviness,” *Composite structures*, vol. 93, no. 9, pp. 2400–2408, 2011.

[45] M. R. Garnich and G. Karami, “Localized fiber waviness and implications for failure in unidirectional composites,” *Journal of composite materials*, vol. 39, no. 14, pp. 1225–1245, 2005.

[46] G. B. Murri, “Influence of ply waviness on fatigue life of tapered composite flexbeam laminates,” In *Composite Structures: Theory and Practice*. ASTM International, 2001.

[47] D. O. Adams and S. J. Bell, “Compression strength reductions in composite laminates due to multiple-layer waviness,” *Composites science and Technology*, vol. 53, no. 2, pp. 207–212, 1995.

[48] S. T. Pinho, L. Iannucci, and P. Robinson, “Physically-based failure models and criteria for laminated fibre-reinforced composites with emphasis on fibre kinking : Part I : Development,” *Composites Part A: Applied Science and Manufacturing,* vol. 37, no. 1, pp. 63–73, 2006.

[49] R. Gutkin, S. T. Pinho, P. Robinson, and P. T. Curtis, "Micro-mechanical modelling of shear-driven fibre compressive failure and of fibre kinking for failure envelope generation in CFRP laminates," *Composites Science and Technology*, vol. 70, no. 8, pp. 1214–1222, 2010.

[50] W. S. Slaughter and N. A. Fleck, "Microbuckling of fiber composites with random initial fiber waviness," *Journal of the Mechanics and Physics of Solids,* vol. 42, no. 11, pp. 1743–1766, 1994.

[51] M. R. Wisnom, "Analysis of shear instability in compression due to fibre waviness," *Journal of reinforced plastics and composites,* vol. 12, no. 11, pp. 1171–1189, 1993.

[52] H. J. Chun, J. Y.Shin, and I. M. Daniel, "Effects of material and geometric nonlinearities on the tensile and compressive behavior of composite materials with fiber waviness," *Composites Science and Technology*, vol. 61, no 1, pp. 125–134, 2001.

[53] A. Beakou, M. Cano, J. B. Le Cam, and V. Verney, "Modelling slit tape buckling during automated prepreg manufacturing: A local approach," *Composite structures*, vol. 93, no. 10, pp. 2628–2635, 2011.

[54] M. Y. Matveev, P. J. Schubel, A. C. Long, and I. A. Jones, "Understanding the buckling behaviour of steered tows in Automated Dry Fibre Placement (ADFP)," *Composites Part A: Applied Science and Manufacturing*, vol. 90, pp. 451–456, 2016.

[55] R. Wehbe, B. Tatting, S. Rajan, R. Harik, M. Sutton, and Z. Gürdal, "Geometrical modeling of tow wrinkles in automated fiber placement," *Composite Structures.*, vol. 246, 2020.

[56] M. Belhaj and M. Hojjati, “Wrinkle formation during steering in automated fiber placement: Modeling and experimental verification,” *Journal of Reinforced Plastics and Composites*, vol. 37, no. 6, pp. 396–409, 2018.

[57] S. Rajan, M. A. Sutton, R. Wehbe, B. Tatting, Z. Gürdal, A. Kidane,and R. Harik., “Experimental investigation of prepreg slit tape wrinkling during automated fiber placement process using StereoDIC,” *Composites Part B: Engineering*, vol. 160, pp. 546–557, 2019.

[58] N. Bakhshi, *Process-induced defects during tow steering in automated fiber placement: experiment, modeling and simulation*, Master’s thesis, Concordia University, 2018.

[59] T. Ondarcuhu, “Tack of a polymer melt: adhesion measurements and fracture profile observations,” *Journal de Physique II*, vol. 7, no 12, pp. 1893–1916, 1997.

[60] K. J. Ahn, J. C. Seferis, T. Pelton, and M. Wilhelm, “Analysis and characterization of prepreg tack,” *Polymer Composites*, vol. 13, no. 3, pp. 197–206, 1992.

[61] D. Budelmann, C. Schmidt, and D. Meiners, “Prepreg tack: A review of mechanisms, measurement, and manufacturing implication,” *Polymer Composites*, vol. 41, no. 9, pp. 3440–3458, 2020.

[62] O. Dubois, J. B. Le Cam, and A. Béakou, “Experimental analysis of prepreg tack,” *Experimental Mechanics*, vol. 50, no. 5, pp. 599–606, 2010.

[63] A. M. Gillanders, S. Kerr, and T. J. Martin, “Determination of prepreg tack,” *International Journal of Adhesion and Adhesives*, vol. 1, no. 3, pp. 125–134, 1981.

[64] C. Wohl, F. L. Palmieri, A. Forghani, C. Hickmott, H. Bedayat, B. Coxon, A. Poursartip,

and B. Grimsley, “Tack measurements of prepreg tape at variable temperature and humidity.” 2017.

[65] S. Rao, R. Umer, J. Thomas, and W. J. Cantwell, “Investigation of peel resistance during the fibre placement process,” *Journal of Reinforced Plastics and Composites*, vol. 35, no. 4, pp. 275–286, 2016.

[66] R. Banks, A. P. Mouritz, S. John, F. Coman, and R. Paton, “Development of a new structural prepreg: Characterisation of handling, drape and tack properties,” *Composite structures*, vol. 66, no. 1–4, pp. 169–174, 2004.

[67] R. J. Crossley, P. J. Schubel, and N. A. Warrior, “The experimental determination of prepreg tack and dynamic stiffness,” *Composites Part A: Applied Science and Manufacturing*, vol. 43, no. 3, pp. 423–434, 2012.

[68] R. J. Crossley, P. J. Schubel, and N. A. Warrior, “Experimental determination and control of prepreg tack for automated manufacture,” *Plastics, rubber and composites*, vol. 40, no. 6–7, pp. 363–368, 2011.

[69] A. Endruweit, G.Y. Choong, S. Ghose, B.A. Johnson, D.R. Younkin, N.A. Warrior, and D.S.A. De Focatiis, “Characterisation of tack for uni-directional prepreg tape employing a continuous application-and-peel test method,” *Composites Part A: Applied Science and Manufacturing*, vol. 114, pp. 295–306, 2018.

[70] R. J. Crossley, P. J. Schubel, and D. S. A. De Focatiis, “Time-temperature equivalence in the tack and dynamic stiffness of polymer prepreg and its application to automated composites manufacturing,” *Composites Part A: Applied science and manufacturing*, vol. 52, pp. 126–133, 2013.

[71] Z. Giirdal and R. Olmedot, “In-plane response of laminates with spatially varying fiber orientations : variable stiffness concept,” *AIAA journal,* vol. 31, no. 4, pp. 751–758, 1993.

[72] S. Setoodeh, M. M. Abdalla, and Z. Gürdal, “Design of variable-stiffness laminates using lamination parameters,” *Composites Part B: Engineering*, vol. 37, no. 4-5, pp. 301–309, 2006.

[73] Z. Gu, B. F. Tatting, and C. K. Wu, “Variable stiffness composite panels : Effects of stiffness variation on the in-plane and buckling response,” *Composites Part A: Applied Science and Manufacturing,* vol. 39, no. 5, pp. 911–922, 2008.

[74] P. Hörmann, *Thermoset automated fibre placement – on steering effects and their prediction*. Institute for Carbon Composites, 2015.

[75] A. D. Kerr, “Elastic and viscoelastic foundation models,” *Journal of Applied Mechanics,* vol. 31, no. 3, pp. 491–498, 1964.

[76] I. E. Avramidis and K. Morfidis, “Bending of beams on three-parameter elastic foundation,” *International Journal of Solids and Structures* vol. 43, no. 2, pp. 357–375, 2006.

[77] U. S. Gupta, A. H. Ansari, and S. Sharma, “Buckling and vibration of polar orthotropic circular plate resting on Winkler foundation,” *Journal of sound and vibration*, vol. 297, no. 3-5, pp. 457–476, 2006.

[78] C. Kassapoglou, *Design and Analysis of Composite Structures.* John Wiley & Sons, Ltd, 2010.

[79] J. N. Reddy, *Theory and Analysis of Elastic Plates and Shells.* Taylor & Francis Group,

LLC, 2007.

[80] B. N. Singh, A. Lal, and R. Kumar, “Post buckling response of laminated composite plate on elastic foundation with random system properties,” *Communications in Nonlinear Science and Numerical Simulation,* vol. 14, no. 1, pp. 284–300, 2009.

[81] M. J. Robert, *Buckling of Bars,Plates, and shells.* Bull Ridge, 2006.

[82] H. Alshahrani, R. Mohan, and M. Hojjati, “Experimental investigation of in-plane shear deformation of out-of-autoclave prepreg,” *International Journal of Composite Materials,* vol. 5, no. 4, pp. 81–87, 2015.

[83] P. Boisse, N. Hamila, E. Guzman-Maldonado, A. Madeo, G. Hivet, and F. Dell’Isola, “The bias-extension test for the analysis of in-plane shear properties of textile composite reinforcements and prepregs : a review,” *International Journal of Material Forming,* vol. 10, no. 4, pp. 473–492, 2017.

[84] Q. Zhang, G. A. O. Qiang, and C. A. I. Jin, “Experimental and simulation research on thermal stamping of carbon fiber composite sheet,” *Transactions of Nonferrous Metals Society of China,* vol. 24, no. 1, pp. 217–223, 2014.

[85] Cytec Engineered Materials . CYCOM 977-2. Product data sheet, December 2013.

[86] Q. Chu, Y. Li, J. Xiao, D. Huan, and X. Chen, “Modeling and experimental investigation of out-of-plane deformation on mechanical performance of composites manufactured by ATL,” *Journal of Reinforced Plastics and Composites,* vol. 36, no. 5, pp. 347–359, 2017.

[87] D. C. Nguyen and C. Krombholz, “Influence of process parameters and material aging on the adhesion of prepreg in AFP processes,” in *17th European Conference on Composite*

Materials, 2012.

[88] A. Endruweit, S. Ghose, B. A. Johnson, S. Kelly, D. S. A. De Focatiis, and N. A. Warrior, "Tack testing to aid optimisation of process parameters for automated material placement in an industrial environment," in *Annual International Conference on Composite Materials (ICCM 21). 2017*.

[89] A. W. Smith, A. Endruweit, G. Y. H. Choong, D. S. A. De Focatiis, and P. Hubert, "Adaptation of material deposition parameters to account for out-time effects on prepreg tack," *Composites Part A: Applied Science and Manufacturing*, vol. 133, 2019.

[90] N. Bakhshi and M. Hojjati, "Effect of compaction roller on layup quality and defects formation in automated fiber placement," *Journal of Reinforced Plastics and Composites*, vol. 39, no. 1–2, pp. 3–20, 2020.

[91] N. Bakhshi and M. Hojjati, "An experimental and simulative study on the defects appeared during tow steering in automated fiber placement," *Composites Part A: Applied Science and Manufacturing*, vol. 113, pp. 122–131, 2018.

[92] D. Budelmann, H. Detampel, C. Schmidt, and D. Meiners, "Interaction of process parameters and material properties with regard to prepreg tack in automated lay-up and draping processes," *Composites Part A: Applied Science and Manufacturing*, vol. 117, pp. 308–316, 2019.

[93] L. Zhang and J. Wang, "A generalized cohesive zone model of the peel test for pressure-sensitive adhesives," *International journal of adhesion and adhesives*, vol. 29, no. 3, pp. 217–224, 2009.

[94] ASTM D 6862-04. Standard test method for 90 degree peel resistance of adhesives. ASTM International; 2004.

[95] M. N. Islam and A. Pramanik, "Comparison of design of experiments via traditional and taguchi method," *Journal of Advanced Manufacturing Systems*, vol. 15, no. 3, pp. 151–160, 2016.

[96] G. Taguchi, S. Konishi, *Taguchi methods, orthogonal arrays and linear graphs-Tools for quality engineering*. American Supplier Institute, Inc. 1987.

[97] W. Ferdous, A. Manalo, and T. Aravinthan, "Bond behaviour of composite sandwich panel and epoxy polymer matrix: Taguchi design of experiments and theoretical predictions," *Construction and Building Materials*, vol. 145, pp. 76–87, 2017.

Appendix A

- Derivation of critical steering radius R_{cr}

Equation 3.13 is differentiated with respect to wavelength L

$$\frac{\partial P_{cr}}{\partial L} = -48D_{11}\frac{\pi^2 m^2}{L^3} + 180D_{22}\frac{L}{\pi^2 m^2 b^4} + 9k\frac{L}{\pi^2 m^2} + 60G\frac{L}{\pi^2 m^2 b^2} = 0$$

This equation then divided by L

$$-48D_{11}\frac{\pi^2 m^2}{L^4} + 180D_{22}\frac{1}{\pi^2 m^2 b^4} + 9k\frac{1}{\pi^2 m^2} + 60G\frac{1}{\pi^2 m^2 b^2} = 0$$

$$L^4 = \frac{48D_{11}\pi^4 m^4 b^4}{180D_{22} + 9kb^4 + 60Gb^2}$$

$$L^2 = \frac{4\pi^2 m^2 b^2\sqrt{3D_{11}}}{\sqrt{180D_{22} + 9kb^4 + 60Gb^2}}\left(\frac{\sqrt{D_{11}}}{\sqrt{D_{11}}}\right) = \frac{4\sqrt{3}D_{11}\pi^2 m^2 b^2}{\sqrt{D_{11}(180D_{22} + 9kb^4 + 60Gb^2)}}$$

$$I = \sqrt{D_{11}(180D_{22} + 9kb^4 + 60Gb^2)}$$

By substituting L^2 in Equation 3.13, we can get P_{min}

$$P_{min} = \frac{1}{6-\alpha}\left[\frac{6D_{11}\pi^2 m^2 I}{\pi^2 m^2 b^2\sqrt{3}D_{11}} + \frac{40(4D_{66} - D_{12})}{b^2} + \frac{360D_{22}\pi^2 m^2 b^2\sqrt{3}D_{11}}{\pi^2 m^2 b^4 I}\right.$$
$$\left. + \frac{18k\pi^2 m^2 b^2\sqrt{3}D_{11}}{\pi^2 m^2 I} + 6G + \frac{120G\pi^2 m^2 b^2\sqrt{3}D_{11}}{\pi^2 m^2 b^2 I}\right]$$

$$P_{min} = \frac{2}{6-\alpha}\left[\frac{360\sqrt{3}D_{22}D_{11} + 18\sqrt{3}kb^4 D_{11} + 120\sqrt{3}Gb^2 D_{11} + 2I(40D_{66} - 10D_{12}) + 3Gb^2 I}{b^2 I}\right]$$

By solving this equation with the steering load (equation 3.14), we can get R_{cr}

$$R_{cr} = \frac{(6-\alpha)Ehb^3 I}{2\alpha\left[360\sqrt{3}D_{22}D_{11} + 18\sqrt{3}kb^4 D_{11} + 120\sqrt{3}Gb^2 D_{11} + 2I(40D_{66} - 10D_{12}) + 3Gb^2 I\right]}$$

- Derivation of wrinkle wavelength L

The wrinkle wavelength is derived by solving the two loads in equations 3.13 and 3.14.

$$(6-\alpha)\left(\frac{Ehb}{R\alpha}\right) = \begin{array}{r} 24D_{11}\left(\frac{\pi m}{L}\right)^2 + 160D_{66}\frac{1}{b^2} - 40D_{12}\frac{1}{b^2} + 90D_{22}\left(\frac{L}{\pi m b^2}\right)^2 \\ + \frac{9}{2}k\left(\frac{L}{\pi m}\right)^2 + G\left(30\left(\frac{L}{\pi m b}\right)^2 + 6\right) \end{array}$$

This equation is multiplied by L^2

$$(6-\alpha)\left(\frac{Ehb}{R\alpha}\right)L^2 = \begin{array}{r} 24D_{11}(\pi m)^2 + 160D_{66}\frac{L^2}{b^2} - 40D_{12}\frac{L^2}{b^2} + 90D_{22}\left(\frac{1}{\pi m b^2}\right)^2 L^4 \\ + \frac{9}{2}k\left(\frac{1}{\pi m}\right)^2 L^4 + 6GL^2 + 30G\left(\frac{1}{\pi m b}\right)^2 L^4 \end{array}$$

$$(6-\alpha)\left(\frac{Ehb}{R\alpha}\right)L^2$$

$$= L^4\left[90D_{22}\left(\frac{1}{\pi m b^2}\right)^2 + \frac{9}{2}k\left(\frac{1}{\pi m}\right)^2 + 30G\left(\frac{1}{\pi m b}\right)^2\right]$$

$$+ L^2\left[160D_{66}\left(\frac{1}{b^2}\right) - 40D_{12}\left(\frac{1}{b^2}\right) + 6G\right] + 24D_{11}(\pi m)^2$$

Finally, wrinkle wavelength can be determined by solving this biquadratic equation 3.18.

Appendix B

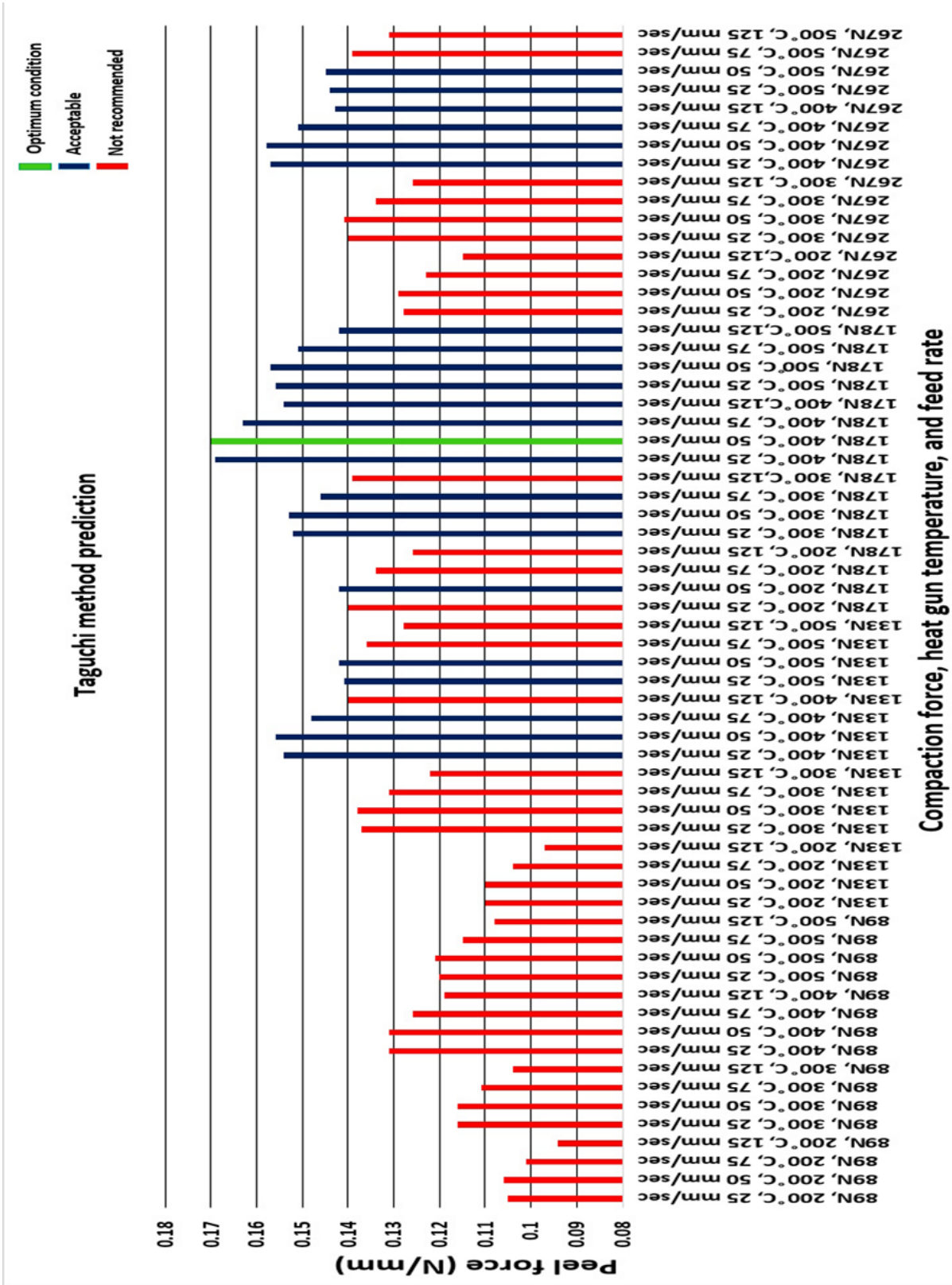
Optimum condition
Acceptable
Not recommended
Taguchi method prediction
Peel force (N/mm)
0.18
0.17
0.16
0.15
0.14
0.13
0.12
0.11
0.1
0.09
0.08
Compaction force, heat gun temperature, and feed rate
89N, 200°C, 25 mm/sec
89N, 200°C, 50 mm/sec
89N, 200°C, 75 mm/sec
89N, 200°C, 125 mm/sec
89N, 300°C, 25 mm/sec
89N, 300°C, 50 mm/sec
89N, 300°C, 75 mm/sec
89N, 300°C, 125 mm/sec
89N, 400°C, 25 mm/sec
89N, 400°C, 50 mm/sec
89N, 400°C, 75 mm/sec
89N, 400°C, 125 mm/sec
89N, 500°C, 25 mm/sec
89N, 500°C, 50 mm/sec
89N, 500°C, 75 mm/sec
89N, 500°C, 125 mm/sec
133N, 200°C, 25 mm/sec
133N, 200°C, 50 mm/sec
133N, 200°C, 75 mm/sec
133N, 200°C, 125 mm/sec
133N, 300°C, 25 mm/sec
133N, 300°C, 50 mm/sec
133N, 300°C, 75 mm/sec
133N, 300°C, 125 mm/sec
133N, 400°C, 25 mm/sec
133N, 400°C, 50 mm/sec
133N, 400°C, 75 mm/sec
133N, 400°C, 125 mm/sec
133N, 500°C, 25 mm/sec
133N, 500°C, 50 mm/sec
133N, 500°C, 75 mm/sec
133N, 500°C, 125 mm/sec
178N, 200°C, 25 mm/sec
178N, 200°C, 50 mm/sec
178N, 200°C, 75 mm/sec
178N, 200°C, 125 mm/sec
178N, 300°C, 25 mm/sec
178N, 300°C, 50 mm/sec
178N, 300°C, 75 mm/sec
178N, 300°C,125 mm/sec
178N, 400°C, 25 mm/sec
178N, 400°C, 50 mm/sec
178N, 400°C, 75 mm/sec
178N, 400°C,125 mm/sec
178N, 500°C, 25 mm/sec
178N, 500°C, 50 mm/sec
178N, 500°C, 75 mm/sec
178N, 500°C,125 mm/sec
267N, 200°C, 25 mm/sec
267N, 200°C, 50 mm/sec
267N, 200°C, 75 mm/sec
267N, 200°C,125 mm/sec
267N, 300°C, 25 mm/sec
267N, 300°C, 50 mm/sec
267N, 300°C, 75 mm/sec
267N, 300°C, 125 mm/sec
267N, 400°C, 25 mm/sec
267N, 400°C, 50 mm/sec
267N, 400°C, 75 mm/sec
267N, 400°C, 125 mm/sec
267N, 500°C, 25 mm/sec
267N, 500°C, 50 mm/sec
267N, 500°C, 75 mm/sec
267N, 500°C, 125 mm/sec